

Optimization of IRS-aided Sub-THz Communications under practical design constraints

Alberto Tarable, Francesco Malandrino *Senior Member, IEEE*, Laura Dossi,
Roberto Nebuloni, Giuseppe Virone, *Senior-Member, IEEE*,
Alessandro Nordio, *Member, IEEE*

Abstract

We consider the optimization of a smart radio environment where meta-surfaces are employed to improve the performance of multiuser wireless networks working at sub-THz frequencies. Motivated by the extreme sparsity of the THz channel we propose to model each meta-surface as an electronically steerable reflector, by using only two parameters, regardless of its size. This assumption, although suboptimal in a general multiuser setup, allows for a significant complexity reduction when optimizing the environment and, despite its simplicity, is able to provide high communication rates. We derive a set of asymptotic results providing insight on the system behavior when both the number of antennas at the transmitter and the meta-surfaces area grow large. For the optimization we propose an algorithm based on the Newton-Raphson method and a simpler, yet effective, heuristic approach based on a map associating meta-surfaces and users. Through numerical results we provide insights on the system behavior and we assess the performance limits of the network in terms of supported users and spatial density of the meta-surfaces.

Index Terms

Intelligent Reflecting Surfaces, Multiuser channel, optimization, TeraHertz communications.

I. INTRODUCTION

The recent advent of the fifth generation (5G) of wireless mobile communications is revolutionizing the way we live and work, thanks to the massive increase of network capacity, to

A. Tarable, F. Malandrino, L. Dossi, R. Nebuloni, G. Virone, A. Nordio are with the National Research Council of Italy, Institute of Electronics, Information Engineering and Telecommunication (CNR-IEIIT), 10129 Torino, Italy (e-mail: <name>.<surname>@ieiit.cnr.it).

its ultra-low latency, and the possibility to connect hundreds of billions of devices. To achieve this goal, millimeter wave (mm-wave) communications combined with massive multiple-input multiple-output (mMIMO) techniques have been advocated for boosting the bandwidth and the spectral efficiency, respectively. It is also expected that the future generation of mobile communications (6G) will exploit sub-THz/THz frequency bands (0.1—10 THz) [1], [2] for indoor as well as outdoor applications involving both static and mobile users, and when very high data rates are required over short distances. However, such frequencies suffer from high path loss, harsh propagation conditions, and blockages.

An innovative solution to overcome the shortcoming of THz bands is defined by the umbrella term of smart radio environment (SRE) [3]. SRE is a dynamically configured environment, where the interaction between radio waves and objects can be controlled in a programmable way. By considering the propagation characteristics of the environment as an exploitable resource rather than a source of signal degradation, SRE can potentially revolutionize the classical paradigm of wireless networking. One of the most promising and realistic implementations of SRE makes use of software-defined intelligent reflecting surfaces (IRSs) [4], which could be integrated within the walls of a room or of a building. An IRS is a two-dimensional *meta-surface*, composed of a large array of passive or active scattering elements, called *meta-atoms* [5], [6], with a specifically designed physical structure and radiation pattern. Meta-surfaces can control, in a software-defined manner, the phase shifts applied by individual meta-atoms to the incident waves. By smartly adjusting such phase shifts, the reflected signals can be either coherently combined at the intended receiver to increase the received power, or destructively combined at non-intended receivers to mitigate interference, thus realizing an energy-efficient beamforming, allowing high performance with lower transmission power. When the line-of-sight (LoS) link between the transmitter and the receiver is absent or severely degraded, connectivity can still be granted by pointing narrow radio beams towards an IRS in LoS and configure it to point to the receiver, as exemplified in Fig. 1. An overview of principles and challenges of IRSs for wireless communications can be found in [7], whereas [8] provides an extensive review ranging from their physical characterization to the discussion of design methodologies and existing prototypes and their applications to wireless communications. Also, [9] elaborates on aspects such as passive reflection optimization, channel estimation, and deployment from various communication perspectives. It is expected that IRSs will become key actors in future wireless networks, by synergically interoperating with other network control strategies and signal processing techniques [10], [11], [12]. By realizing the SRE paradigm, IRSs can make THz

communication technologies viable for application in a large class of indoor and outdoor scenarios, as envisioned by current 5G and future 6G standards [5], [13], [14]. Moreover, IRSs allow to move part of the intelligence of the system from the transceivers to the environment, while improving the spectrum-sharing capacity in multiuser communications, as shown in [15]. IRSs can be applied to a wide range of propagation scenarios, ranging from GHz to THz frequencies [16]. In the GHz bands, channels are characterized by rich scattering, so that the radio links from/to each IRS element are assumed to undergo independent fading. In such a situation, the phase shifts applied by the IRS elements need to be jointly optimized according to some figure of merit, such as network throughput. Typical solutions from the literature resort to, e.g., alternating optimization, as done in [17], [18]. Such approach, however, requires the estimation of large channel matrices with independent entries, entailing communication overhead. Moreover, its complexity increases with the number of IRS elements [10], [11], [19], [20], [17]. The picture changes dramatically for systems operating in the sub-THz/THz frequency bands. Indeed, although the wireless channel at such frequencies is not yet completely characterized, it is known that it becomes sparser and its main components are the LoS and some non-LoS (NLoS) reflected rays, while scattering and diffraction provide little contribution to the received signal power [21], [22], [23]. Moreover, if beamforming is employed and the signal power is concentrated in a specific direction, the effect of multipath is further reduced. In such a scenario IRS can be more easily optimized and they can be configured to macroscopically act as programmable mirrors.

A. *Novelties and contributions*

In this work, we pose the following questions: in a sub-THz communication system, how efficient a simple optimization of IRS phase shifts could be? Or, more precisely, what performance is achievable when the optimization algorithm treats the whole IRS as a single mirror-like entity, as opposed to a mere collection of meta-atoms? We anticipate the surprising answer: in some conditions, simplicity and optimality are not incompatible.

To answer these questions we consider the downlink of a wireless network where a base station (BS) communicates with a set of K randomly placed user equipments (UEs) through N IRSs. There is no direct path from the BS to the UEs, however a NLoS path exists between them, due to the reflection from a large wall. Both the BS and the UE are equipped with arrays of antennas so that they are able to apply beamforming techniques. While the BS antenna array can perform digital beamforming, we consider a practical scenario where,

due to limited UE cost, the UEs antenna array can only allow for analog beamforming. The scenario is depicted in Fig. 1.

We adopt a sparse channel model, typical of sub-THz/THz frequencies where multipath is due to few reflectors (e.g., large static objects, such as walls) and the path loss is characterized by both large-scale fading and molecular absorption.

We consider the IRS model in [24], and since used by several authors [25], [26], [27] which describes an IRS as an array of subwavelength-sized diffuse scatterers which phase-align their reflected signals in a specified direction in order to achieve “anomalous” reflection properties. The phase shifts applied by the meta-atoms are related to each other through a linear equation. Finally, each IRS is characterized by two design parameters, regardless of the number of meta-atoms, namely:

- a constant *phase gradient* among the IRS elements, which, according to the generalized Snell’s law [24], determines the *steering angle* applied by the IRS to the impinging signal;
- a *phase shift*, which adjusts the phase of the signal reflected by each IRS in order to constructively/destructively interfere with other desired/undesired signals at the UE end.

Such IRS model is known to be optimal for a single-user system in pure LoS IRS-UE channels although it is suboptimal for a multi-user systems characterized by multipath channels. Nevertheless, it has several advantages: first of all, each IRS can be characterized by only two parameters, hence the complexity of the optimization process is significantly reduced. Secondly, the estimation and exchange of a large number of channel coefficients, one for each IRS element, is not required, as the system only needs the knowledge of the positions of the UEs to serve. Also, it allows for the design of efficient SRE optimization algorithms which, in a wide range of relevant conditions, are equivalent to a smart one-to-one association between UEs and IRSs, as shown later. In fact, for highly directive beams, as is the case in sub-THz and THz applications, when IRSs are optimally configured to serve a certain UE, due to the asymptotic orthogonality among channel vectors associated with different users, IRSs will become interference-free to other users [20]. Finally, the optimality of the model in [24] also holds for several multiuser setups, as shown later.

Our main contributions can be summarized as follows:

- we analyze the performance of the downlink in a practical IRS-aided multi-user network operating in the sub-THz frequency band, where the direct BS-US LoS path is blocked and multipath components are due to reflection on few large static objects;

- we formulate an SRE optimization problem, considering a case in which the BS performs zero-forcing (ZF) precoding, the performance metric is the received signal-to-noise ratio (SNR) at the UEs, and the optimization variables are the phase gradients and the phase shifts for all IRSs, as well as the steering directions of the UEs antenna arrays;
- we propose a simple and efficient heuristic solution, based on the Hungarian algorithm, which associates a IRS to each user; we then analytically show that this approach becomes essentially optimal in the asymptotic regime where the IRSs areas are large and the BS array has a large number of antennas;
- through numerical analysis, we highlight the role of the network design parameters and their effects on the system performance; in particular (i) we assess the contribution to the received SNR due to NLoS components, (ii) we verify the optimality of the heuristic approach in realistic conditions, (iii) we assess the performance loss incurred when discrete phase-shifters are employed and (iv) we provide design rules for the sizing of the system, in order to be able to fully exploit the degrees of freedom that are intrinsically available in a reference scenario;

Beyond taking into account several aspects that are most often overlooked in the literature (reflection by large static objects, multiple antennas at the UEs), the novelty in the paper resides in the proposal of an efficient, *practical* way of performing SRE optimization, compatible with the low delay required by near-real-time scenarios, and in the analysis of its performance, whose understanding paves the way for the implementation of a veritable IRS-assisted quasi-orthogonal space-division multiple access.

The reminder of the paper is organized as follows. In Section II, we introduce the communication model and characterize the IRSs. In Section III, we provide an asymptotic expression of the channel matrix. Section IV derives the relation between the phase gradient applied to the IRS and the resulting electronic rotation angle. Section V proposes a set of algorithms for SRE optimization, while Section VI discusses the sensitivity of such algorithms to network parameters. Finally, Section VII provides a set of numerical results obtained by applying the proposed algorithms to a realistic environment. Conclusions are drawn in Section VIII.

B. Mathematical notation

Boldface uppercase and lowercase letters denote matrices and vectors, respectively. \mathbf{I}_k is the $k \times k$ identity matrix and $\mathbf{1}_k$ is the all-1 column vector of length k . The conjugate transpose of matrix \mathbf{A} is denoted by \mathbf{A}^H , while $[\mathbf{A}]_{i,j}$ is its (i, j) -th element. \mathbf{A}^+ and $\|\mathbf{A}\|_F$ refer, respectively, to the Moore-Penrose pseudo-inverse and the Frobenius norm of \mathbf{A} . The notation

$\mathbf{A} = \text{diag}(\mathbf{a})$ specifies that the entries of the vector \mathbf{a} are the elements of the diagonal matrix \mathbf{A} . Symbols \otimes and $\mathbb{E}[\cdot]$ denote the Kronecker product and the average operator, respectively. Finally, we define the norm-1 length- M column vector $\mathbf{s}(\Delta, M, \beta)$, whose m -th entry is

$$[\mathbf{s}(\Delta, M, \beta)]_m = \frac{1}{\sqrt{M}} e^{j\pi\Delta(M-1)\sin\beta} e^{-j2\pi\Delta(m-1)\sin\beta} \quad (1)$$

for $m = 0, \dots, M-1$. This vector represents the (normalized) spatial signature of a uniform linear array (ULA) composed of M elements spaced by Δ wavelengths as observed from the angle β , measured from the normal to the ULA.

II. COMMUNICATION MODEL

We consider the downlink of a wireless network operating in the sub-THz band. The network is composed of a BS, which transmits K data streams to K users (UEs). We assume that the UEs are not in LoS with the BS. Nevertheless, they can receive the BS signal through a NLoS reflection provided by a wall and through a set of N IRS, as depicted in Fig. 1. In order to simplify the discussion and the mathematical description of the system, we assume that transceivers, IRSs and reflectors have the same height above ground (2D model), so that all the relevant angles lie on the azimuth plane¹. In the following we provide a detailed description of the BS, the IRSs and the UEs, as well as of the channel model.

A. Base Station

The BS is equipped with an ULA composed of M_1 isotropic antennas, spaced by Δ_1 wavelengths. Thus, the transmitted signal, \mathbf{t} , can be represented by the $M_1 \times 1$ vector

$$\mathbf{t} = \mathbf{\Gamma}\mathbf{x}, \quad (2)$$

where $\mathbf{x} = [x_1, \dots, x_K]^T$ is the vector of transmitted symbols for the K users, supposed to have zero mean and covariance $\mathbb{E}[\mathbf{x}\mathbf{x}^H] = \mathbf{I}_K$, and $\mathbf{\Gamma}$ is a precoding matrix. We assume that the transmit power cannot exceed \mathcal{P}_t , i.e.,

$$\mathbb{E}[\|\mathbf{t}\|_2^2] = \mathbb{E}_{\mathbf{x}} [\|\mathbf{\Gamma}\mathbf{x}\|_2^2] = \|\mathbf{\Gamma}\|_F^2 \leq \mathcal{P}_t. \quad (3)$$

¹The extension to a 3D scenario is straightforward and does not add significant insight on the system behavior.

B. User Equipments

At the receiver side, we assume that the UEs are equipped with ULAs as well. Specifically, each UE ULA is composed of M_2 isotropic antennas spaced by Δ_2 wavelengths. Hence, the signal received by the k -th UE can be described by the $M_2 \times 1$ vector

$$\mathbf{r}_k = \tilde{\mathbf{H}}_k \mathbf{t} + \mathbf{z}_k, \quad (4)$$

where $\tilde{\mathbf{H}}_k$ is the $M_2 \times M_1$ channel matrix connecting the BS to the k -th UE, \mathbf{t} is given by (2), and \mathbf{z}_k is a vector of i.i.d. complex, circularly symmetric Gaussian noise random variables with zero mean and variance σ^2 . We assume that the UE ULAs can only perform analog beamforming, since they are supposed to have limited hardware complexity. Thus, the k -th UE applies to \mathbf{r}_k the beamforming vector $\mathbf{f}_k = \mathbf{s}(\Delta_2, M_2, \alpha_k)$ and forms the output

$$y_k = \mathbf{f}_k^H \mathbf{r}_k = \mathbf{f}_k^H \tilde{\mathbf{H}}_k \mathbf{t} + \eta_k, \quad (5)$$

where $\eta_k = \mathbf{f}_k^H \mathbf{z}_k$ is a complex Gaussian random variable with zero mean and variance σ^2 , and α_k is the direction of the k -th UE beam, measured from the direction normal to the UE ULA. In conclusion, the signal received by the K UEs can be described by the vector

$$\mathbf{y} = \begin{bmatrix} y_1 \\ \vdots \\ y_K \end{bmatrix} = \underbrace{\begin{bmatrix} \mathbf{f}_1^H \tilde{\mathbf{H}}_1 \\ \vdots \\ \mathbf{f}_K^H \tilde{\mathbf{H}}_K \end{bmatrix}}_{\tilde{\mathbf{H}}} \mathbf{t} + \boldsymbol{\eta}, \quad (6)$$

where $\tilde{\mathbf{H}}$ is the overall channel matrix and $\boldsymbol{\eta} = [\eta_1, \dots, \eta_K]^T$.

C. Sub-THz communication channel

1) *Single-hop channel model:* At sub-THz/THz frequencies, the wireless channel has not been completely characterized yet. We know that the main components are the LoS and NLoS reflected rays while scattering and diffraction provide marginal contribution [21], [22]. Moreover, the number of multipath (reflected) components is typically very small and even reduces to one when large, high-gain antenna arrays are employed [21]. Furthermore, NLoS paths are subject to severe reflection losses and other important aspects such as molecular absorption, blockage, and large-scale fading effects need to be taken into account.

Then, a single hop link between any two devices equipped with antenna arrays composed of, respectively, p and q elements, can be described by the $p \times q$ matrix [28], [21]

$$\mathcal{H} = \underbrace{a_0 c_0 \mathbf{p}_0 \mathbf{q}_0^H}_{\text{LoS}} + \underbrace{\sum_{p=1}^P a_p c_p \mathbf{p}_p \mathbf{q}_p^H}_{\text{NLoS}}, \quad (7)$$

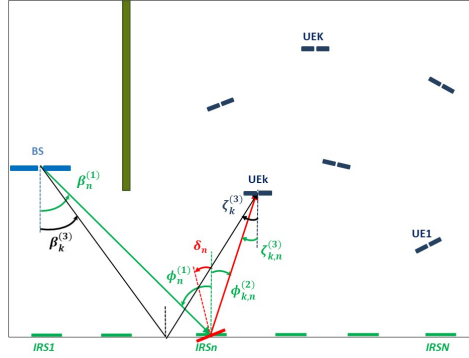


Fig. 1. An example of SRE where a BS communicates with K UEs by exploiting a set of N IRSs deployed along a wall. The direct LoS path between BS and UEs is blocked by an obstacle (dark green block). Green and red solid lines refer to the LoS paths connecting the BS to the n -th IRSs and the n -th IRS to the k -th UE, respectively. The black line denotes the NLoS link connecting the BS with the k -th UE through reflection on a wall (dark thick line at the bottom of the figure).

where the vectors $\mathbf{p}_0 = \mathbf{p}(\varphi_{r,0})$ and $\mathbf{q}_0 = \mathbf{q}(\varphi_{t,0})$ are, respectively, the spatial signatures of the receive and transmit array in the direction of the LoS path, which is observed at the angles $\varphi_{r,0}$ and $\varphi_{t,0}$ by the transmitter and by the receiver, respectively. Moreover, P is the number of NLoS paths, and the vectors $\mathbf{p}_p = \mathbf{p}(\varphi_{r,p})$ and $\mathbf{q}_p = \mathbf{q}(\varphi_{t,p})$, $p = 1, \dots, P$ are the receive and transmit array signatures for the p -th reflector, which is observed at the angles $\varphi_{t,p}$ and $\varphi_{r,p}$. The random variables a_p model large-scale fading whereas c_p account for the attenuation and phase rotation due to propagation. Specifically, we have

$$c_p = \rho_p \sqrt{\frac{G_1 A}{4\pi d_p^2}} e^{-j\frac{2\pi}{\lambda} d_p} e^{-\kappa d_p} = \rho_p \frac{\sqrt{G_1 G}}{4\pi d_p / \lambda} e^{-j\frac{2\pi}{\lambda} d_p} e^{-\kappa d_p}, \quad (8)$$

where ρ_p is the complex reflection coefficient ($\rho_0 = 1$ for the LoS path), d_p is p -th path length and G_1 is the array gain on one side of the link. The first expressions in (8) is employed if the array on the other side is considered in terms of its effective area A , the second expression is preferred if the array is characterized by its gain, G . Finally, the coefficient κ represents the (frequency dependent) molecular absorption coefficient [28], [29].

2) *End-to-end channel model:* In our model the LoS link between the BS and the UEs is blocked by the presence of an obstacle, represented in Fig. 1 by the dark green rectangle. However UEs can receive copies of the BS signal reflected by all IRSs as well as the one reflected by a wall, represented by the dark thick line at the bottom of Fig. 1.

Then, the channel matrix $\tilde{\mathbf{H}}_k$ in (4) can be written as

$$\tilde{\mathbf{H}}_k = \sum_{n=1}^N \mathbf{H}_{k,n}^{(2)} \bar{\Theta}_n \mathbf{H}_n^{(1)} + \mathbf{H}_k^{(3)}, \quad \text{where} \quad (9)$$

- $\mathbf{H}_n^{(1)}$ is the $L_n^2 \times M_1$ channel matrix connecting the BS to the n -th IRS;

- $\bar{\Theta}_n = \mathbf{I}_{L_n} \otimes \Theta_n$ is the diagonal matrix of the phase shifts introduced by the meta-atoms of the n -th IRS, where $\Theta_n = \text{diag}(e^{j\theta_{n,1,1}}, \dots, e^{j\theta_{n,L_n,1}})$, $\theta_{n,\ell,\ell'}$ being defined in (14);
- $\mathbf{H}_{k,n}^{(2)}$ is the $M_2 \times L_n^2$ channel matrix connecting the n -th IRS to the k -th UE;
- $\mathbf{H}_k^{(3)}$ is the channel matrix connecting the BS to the k -th UE, through wall reflection.

In our notation, the superscripts (1) , (2) and (3) refer to the link connecting the BS to the IRSs, the link connecting the IRSs to the UEs, and the path connecting BS and UE through wall reflection, respectively.

Let us first consider the link connecting the BS and the n -th IRS. Since their position is fixed, we assume that they have been conveniently deployed so that they are connected by a dominant unfaded LoS link. Therefore, the channel matrix $\mathbf{H}_n^{(1)}$ in (9) contains only the LoS component and, recalling (7) it can be written as

$$\mathbf{H}_n^{(1)} = c_n^{(1)} \bar{\mathbf{u}}_n^{(1)} \mathbf{v}_n^{(1)H}, \quad \text{where} \quad (10)$$

- $\bar{\mathbf{u}}_n^{(1)} = \frac{1}{\sqrt{L_n}} \mathbf{1}_{L_n} \otimes \mathbf{s}(\Delta, L_n, \phi_n^{(1)})$ is the spatial signature of the n -th IRS and $\phi_n^{(1)}$ is the LoS angle of arrival (AoA) of the BS signal at the n -th IRS, measured with respect to a direction orthogonal to the surface (see Fig. 1);
- $\mathbf{v}_n^{(1)} = \mathbf{s}(\Delta_1, M_1, \beta_n^{(1)})$, where $\beta_n^{(1)}$ is the LoS angle of departure (AoD) of the signal from the BS towards the n -th IRS, measured with respect to the direction orthogonal to the BS ULA;
- $c_n^{(1)} = a_n^{(1)} \frac{\sqrt{M_1 A_n \cos \phi_n^{(1)}}}{\sqrt{4\pi d_n^{(1)}}} e^{-j\frac{2\pi}{\lambda} d_n^{(1)}} e^{-\kappa d_n^{(1)}}$, is the LoS channel gain (8): where A_n is given by (13), and $d_n^{(1)}$ is the distance between the center of the BS ULA and the center of the n -th IRS. We recall that $A_n \cos \phi_n^{(1)}$ is the effective area of the IRS as observed from the AoA $\phi_n^{(1)}$. Finally, since we consider an unfaded LoS link, we set $a_n^{(1)} = 1$.

The IRSs–UEs links are, instead, affected by the random position of the UEs in an environment prone to shadowing effects and potentially containing objects acting as reflectors. Thus, for the link connecting the k -th UE with the n -th IRS we adopt the model in (7) accounting for $P \geq 1$ NLoS paths. The corresponding channel matrix, $\mathbf{H}_{k,n}^{(2)}$, is given by

$$\mathbf{H}_{k,n}^{(2)} = \sum_{p=0}^P a_{k,n,p}^{(2)} c_{k,n,p}^{(2)} \mathbf{w}_{k,n,p}^{(2)} \bar{\mathbf{u}}_{k,n,p}^{(2)H} \quad \text{where} \quad (11)$$

- $a_{k,n,p}^{(2)}$ is a random variable with log-normal distribution, describing large-scale fading effects on the p -th path between the n -th IRS and the k -th UE;
- $\bar{\mathbf{u}}_{k,n,p}^{(2)} = \frac{1}{\sqrt{L_n}} \mathbf{1}_{L_n} \otimes \mathbf{s}(\Delta, L_n, \phi_{k,n,p}^{(2)})$, where $\phi_{k,n,p}^{(2)}$ is the AoD towards the p -th path;
- $\mathbf{w}_{k,n,p}^{(2)} = \mathbf{s}(\Delta_2, M_2, \zeta_{k,n,p}^{(2)})$ is the spatial signature of the k -th UE ULA, as observed from the direction of the p -th path, $\zeta_{k,n,p}^{(2)}$;

- $c_{k,n,p}^{(2)} = \rho_{\text{IRS}} \rho_{k,n,p} \frac{\sqrt{M_2 A_n \cos \phi_{k,n,p}^{(2)}}}{\sqrt{4\pi d_{k,n,p}^{(2)}}} e^{-j\frac{2\pi}{\lambda} d_{k,n,p}^{(2)}} e^{-\kappa d_{k,n,p}^{(2)}}$ is the channel gain of the p -th path, ρ_{IRS} is the IRS reflection coefficient, $\rho_{k,n,p}$ is the reflection coefficient of the p -th reflector, and $d_{k,n,p}^{(2)}$ is the distance between the n -th IRS and the k -th UE, through the p -th path;
- for $p = 0$, the angles $\phi_{k,n,0}^{(2)}$ and $\zeta_{k,n,0}^{(2)}$ refer to the LoS path.

Remark 1: For simplicity we assume the IRS reflection coefficient, ρ_{IRS} , to be a constant independent on the other system parameters. We point out, however, that in some practical settings the amplitude response of a meta-atom depends on the applied phase shift in (14), as observed in [30].

Finally, according to the image theorem, the NLoS link connecting the BS to the k -UEs through reflection on the wall (see Fig. 1) can be described by the matrix

$$\mathbf{H}_k^{(3)} = a_k^{(3)} c_k^{(3)} \mathbf{w}_k^{(3)} \mathbf{v}_k^{(3)H}, \quad \text{where} \quad (12)$$

- $a_k^{(3)}$ is a random variable modeling large scale fading effects;
- $c_k^{(3)} = \rho_{\text{wall}} \frac{\sqrt{M_2 M_1 \lambda^2}}{4\pi d_k^{(3)}} e^{-j\frac{2\pi}{\lambda} d_k^{(3)}} e^{-\kappa d_k^{(3)}}$, where ρ_{wall} is the reflection coefficient of the wall and $d_k^{(3)}$ is the path length;
- $\mathbf{w}_k^{(3)} = \mathbf{s}(\Delta_2, M_2, \zeta_k^{(3)})$ and $\zeta_k^{(3)}$ is the AoA of the signal reflected by the wall, as observed from the k -th UE, from the direction orthogonal to the UE ULA;
- $\mathbf{v}_k^{(3)} = \mathbf{s}(\Delta_1, M_1, \beta_k^{(3)})$, and $\beta_k^{(3)}$ is the AoD of the signal that is reflected by the wall towards the k -th UE, as observed by the BS, measured from the direction orthogonal to the BS ULA.

D. IRS characterization

Radiation pattern. Several power radiation patterns for the IRS elements have been discussed and analyzed in the literature [31]; we here assume that the power of the radiation collected by an IRS of area A is proportional to $A \cos \phi^{(1)}$ for $\phi^{(1)} \in [-\pi/2, \pi/2]$, and zero otherwise, where $\phi^{(1)}$ is the AoA of the radiation. Similarly, we assume that the power radiated by the n -th IRS is proportional to $|\rho_{\text{IRS}}|^2 A \cos \phi^{(2)}$, for $\phi^{(2)} \in [-\pi/2, \pi/2]$ and zero otherwise, where $\phi^{(2)}$ is the AoD of the scattered field and ρ_{IRS} is the reflection efficiency of the IRS. In practice the terms $A \cos \phi^{(1)}$ and $A \cos \phi^{(2)}$ represent the effective area of the IRS when observed from the AoA and AoD, respectively. The above expressions take into account that IRSs typically receive power and radiate it on one side only. Note that in general the IRS's received and radiated powers also depend on the AoA and AoD of the electromagnetic field measured in the elevation plane. However, since we employ a 2D description of the system geometry (i.e. we work in the azimuth plane) such dependencies can be neglected.

We also assume that the intensity of the scattered electromagnetic field decays with the inverse of the distance, and that the IRS are uniformly illuminated by the BS; our model is intended to hold in the far-field regime [32], [24] and when the *angular aperture* of the IRS, as observed from the BS, is small when compared to the beamwidth of the BS signal.

IRS size and phase-shift properties. In our model the n -th IRS, $n = 1, \dots, N$, has square shape and is composed of L_n^2 meta-atoms [5], arranged in a $L_n \times L_n$ square grid, of area

$$A_n = L_n^2 \Delta^2 \lambda^2, \quad (13)$$

where λ is the signal wavelength and Δ is the meta-atom side length, normalized to λ .

The meta-atom at position (ℓ, ℓ') in the n -th surface, $\ell, \ell' = 1, \dots, L_n$, applies a phase shift $\theta_{n,\ell,\ell'}$ to the signal impinging on it. We here assume that such phase shifts can take any value in $[0, 2\pi)$, i.e. the IRS elements behave as continuous phase shifters. However, practical implementations restrict the possible phase shifts to a discrete set, whose cardinality, 2^b , depends on the number of control bits, b , per IRS element. It has been shown that phase shifters with at least 3 control bits entail small performance degradation with respect to continuous phase shifters [33], [34] and achieve close-to-optimal performance.

Many works assume a rich scattering channel and thus optimize the system performance by jointly searching for the appropriate values of each of the phase shifts $\theta_{n,\ell,\ell'}$ [10], [11], [17], [19], [20]. However, as discussed in Section I, since we aim at simplicity and we consider a channel characterized by extreme sparsity and negligible scattering and diffraction effects, we assume that phase shifts of the n -th IRS are related to each other according to the linear equation [25], [26], [27]

$$\theta_{n,\ell,\ell'} = 2\pi g_n \Delta \left(\ell - 1 - \frac{L_n - 1}{2} \right) + \psi_n, \quad (14)$$

for $\ell' = 1 \dots, L_n$. By virtue of (14), the n -th IRS is able to steer the impinging signal and beam it to an arbitrary direction (depending on the parameter g_n , which is proportional to the phase gradient) as well as to apply an arbitrary phase shift, ψ_n , to the reflected signal. Note that (14) allows to characterize the IRS by using only two parameters, i.e., g_n and ψ_n , regardless of the number of meta-atoms, L_n^2 . We point out that, although such IRS model is known to be optimal for a single-user system in pure LoS condition, it allows for a simple, practical and efficient network configuration. Nevertheless, in the following we will show that under particular assumptions, it can be optimal also in a specific multi-user environment. The derivation of a closed form expression of the optimal solution in a general multi-user scenario remains an open problem.

III. ASYMPTOTIC EXPRESSION OF THE CHANNEL MATRIX AND SIGNAL PRECODING

The overall channel matrix $\tilde{\mathbf{H}}$ in (5) can be written in a more tractable form by letting the number of meta-atoms contained in each IRS tend to infinity, while keeping constant the surface area. This is a reasonable assumption since the number of meta-atoms in an IRS is usually large and the normalized meta-atom side length, Δ , is typically very small.

Proposition 1: As $L_1, \dots, L_N \rightarrow \infty$ while the IRS areas A_n remain constant, the matrix $\tilde{\mathbf{H}}$ tends to matrix \mathbf{H} , given by

$$\mathbf{H} = \lim_{L_1, \dots, L_N \rightarrow \infty} \tilde{\mathbf{H}} = \mathbf{M}\Psi\mathbf{V}^{(1)\text{H}} + \mathbf{T}\mathbf{V}^{(3)\text{H}}, \quad (15)$$

where $\Psi = \text{diag}(e^{j\psi_1}, \dots, e^{j\psi_N})$, $\mathbf{V}^{(1)} = [\mathbf{v}_1^{(1)}, \dots, \mathbf{v}_N^{(1)}]$, $\mathbf{V}^{(3)} = [\mathbf{v}_1^{(3)}, \dots, \mathbf{v}_K^{(3)}]$, \mathbf{M} is a $K \times N$ matrix whose elements are given by

$$[\mathbf{M}]_{k,n} = c_n^{(1)} a_{k,n,p}^{(2)} c_{k,n,p}^{(2)} \sum_{p=0}^P b_{k,n,p} \text{sinc}\left(\frac{\sqrt{A_n}}{\lambda} s_{k,n,p}\right), \quad (16)$$

\mathbf{T} is a diagonal matrix whose k -th diagonal element is given by

$$[\mathbf{T}]_{k,k} = b_k a_k^{(3)} c_k^{(3)}, \quad (17)$$

having defined

$$b_{k,n,p} \triangleq \frac{\text{sinc}(\Delta_2 M_2(\sin \alpha_k - \sin \zeta_{k,n,p}))}{\text{sinc}(\Delta_2(\sin \alpha_k - \sin \zeta_{k,n,p}))}, \quad b_k \triangleq \frac{\text{sinc}(\Delta_2 M_2(\sin \alpha_k - \sin \zeta_k))}{\text{sinc}(\Delta_2(\sin \alpha_k - \sin \zeta_k))}, \quad (18)$$

and

$$s_{k,n,p} = \sin \phi_n^{(1)} - \sin \phi_{k,n,p}^{(2)} - g_n. \quad (19)$$

Proof: See Appendix A. ■

We make the following remarks about (16):

- the term $s_{k,n,p}$ is related to the misalignment of the k -th UE w.r.t. the beam generated by the n -th IRS and received through the p -th reflector. We recall that $p = 0$ corresponds to the LoS component between the n -th IRS and the k -th UE. Also, the direction of maximum radiation (for the p -th path) corresponds to $s_{k,n,p} = 0$;
- as it can be expected, (16) is similar to the bistatic radar equation when a tilted flat plate is considered as target;
- each IRS generates a beam whose width is proportional to $\lambda/\sqrt{A_n}$. Therefore, larger surfaces generate narrower beams;
- the channel gain $|[\mathbf{M}]_{k,n}|^2$ is proportional to the square of the product $c_n^{(1)} c_{k,n,p}^{(2)}$ which, in turn, is proportional to the square of the IRS area, A_n^2 ; as observed in [35], such

squared gain shows that the IRSs achieve at the same time a beamforming gain and an aperture gain, both proportional to A_n .

- the term $\text{sinc}\left(\frac{\sqrt{A_n}}{\lambda} s_{k,n,p}\right)$ in (16), is proportional to the radiation pattern of a continuous metal plate with anomalous reflection properties, as observed in [24].

In the following, we will replace the matrix $\tilde{\mathbf{H}}$ with its asymptotic expression \mathbf{H} given in (15), so that, by recalling (2) the received signal takes the form

$$\mathbf{y} = \mathbf{H}\mathbf{\Gamma}\mathbf{x} + \boldsymbol{\eta}. \quad (20)$$

The precoding matrix $\mathbf{\Gamma}$ should be designed so as to adapt the transmitted signal to the propagation environment. Several choices are possible: for example it can be designed to maximize the SINR at the receivers or to null out the interference among UEs, at a price of a reduction of SINR. In this work we consider zero-forcing (ZF) precoding, similarly to what done in [36]. Specifically, we will assume in the following that $\min(M_1, N) \geq K$. Under this hypothesis, we can choose $\mathbf{\Gamma}$ to satisfy

$$\mathbf{H}\mathbf{\Gamma} = a\mathbf{Q}^{1/2}, \quad (21)$$

where \mathbf{Q} is a diagonal matrix and a is a coefficient. Indeed, by substituting (21) in (20) we observe that the effect of the precoder is to diagonalize the end-to-end channel matrix and, by consequence, make the UEs' channels orthogonal. By solving (21) for $\mathbf{\Gamma}$, the precoder can be written as

$$\mathbf{\Gamma} = a\mathbf{H}^+\mathbf{Q}^{1/2}, \quad (22)$$

where $\mathbf{H}^+ = \mathbf{H}^H(\mathbf{H}\mathbf{H}^H)^{-1}$ is the pseudo-inverse of \mathbf{H} and $a = \frac{\sqrt{P_t}}{\|\mathbf{H}^+\mathbf{Q}^{1/2}\|_F}$ in order to meet the transmit power constraint in (3). With this precoder choice, the received SNR at the k -th UE is given by

$$\text{SNR}_k = \frac{P_t q_k}{\sigma^2 \|\mathbf{H}^+\mathbf{Q}^{1/2}\|_F^2}, \quad (23)$$

where q_k is the k -th diagonal element of \mathbf{Q} . The SNR in (23) corresponds to a spectral efficiency per user of

$$R_k = \log_2(1 + \text{SNR}_k), \quad (24)$$

expressed in bit/s/Hz. Note that, by varying q_k it is possible to provide the UEs with different quality of service, i.e., different values of R_k . In the special case $\mathbf{Q} = \mathbf{I}$, all users achieve the same spectral efficiency. While the expression for $\mathbf{\Gamma}$ in (22) is suboptimal in terms of achievable rate, it has the advantage of completely removing interference among streams at the UEs and, more importantly, allows for a relatively simple optimization of the SNR received by the UEs, as shown in Section V.

IV. ELECTRONIC ROTATION OF THE IRSS

The macroscopic effect of the phase gradient applied to the IRS meta-atoms is to *electronically rotate* the IRS with respect to its physical orientation, according to the generalized Snell's law. By electronic rotation, the beam generated by the IRS can be steered to point to an arbitrary direction. The angle of electronic rotation of the n -th IRS, denoted by δ_n (see Fig. 1 for details), only depends on the gradient of the phase shift in (14), i.e. on the parameter g_n . In order to map the parameter g_n into the corresponding rotation angle of the IRS, we make the key observation that the term $s_{k,n,p}$ in (19) can be rewritten as

$$s_{k,n,p} = \sin(\phi_n^{(1)} - 2\delta_n) - \sin(\phi_{k,n,p}^{(2)}), \quad (25)$$

where we recall that the angles $\phi_n^{(1)}$ and $\phi_{k,n,p}^{(2)}$ represent the AoA of the signal received at the n -th IRS and the AoD from the n -th IRS towards the p -th path on the link connecting k -UE, respectively, measured in the azimuth plane and with respect to a direction orthogonal to the surface. Note that the angles $\phi_n^{(1)} - \delta_n$ and $\phi_{k,n,p}^{(2)} + \delta_n$ are the above mentioned AoA and the AoD, respectively, *as seen from the electronically rotated surface*. The relation between the phase gradient, g_n , and the rotation angle, δ_n , can be immediately derived by equating (19) and (25), and is given by $g_n = \sin(\phi_n^{(1)}) - \sin(\phi_n^{(1)} - 2\delta_n)$. In the following, we will drop the expression for $s_{k,n,p}$ in (19) in favor of (25), since the angle δ_n has a clearer geometric interpretation than g_n . Thus, if we want to point the beam generated by the n -th surface in the generic direction $\phi^{(2)}$, we must set the rotation angle δ_n in (25), so as to have $\sin(\phi_n^{(1)} - 2\delta_n) - \sin(\phi^{(2)}) = 0$.

V. SMART RADIO ENVIRONMENT OPTIMIZATION

We now aim at maximizing the SNR in (23), over the variables $\boldsymbol{\delta} = [\delta_1, \dots, \delta_N]^T$, $\boldsymbol{\psi} = [\psi_1, \dots, \psi_N]^T$, and $\boldsymbol{\alpha} = [\alpha_1, \dots, \alpha_K]^T$, characterizing the rotations and phase shifts of the IRSs, and the direction of the beams generated by the UE ULAs, respectively. In practice, for a given matrix \mathbf{Q} , in view of (23), we face the following optimization problem

$$\text{SNR}_k^{\text{opt}} = \max_{\boldsymbol{\xi}} \text{SNR}_k = \frac{\mathcal{P}_t q_k}{\sigma^2 \min_{\boldsymbol{\xi}} \|\mathbf{H}^+ \mathbf{Q}^{1/2}\|_{\text{F}}^2}. \quad (26)$$

where $\boldsymbol{\xi} = [\boldsymbol{\delta}^T, \boldsymbol{\psi}^T, \boldsymbol{\alpha}^T]^T \in [0, 2\pi]^{2N+K}$. As shown in (26), maximizing the SNR is equivalent to minimizing the term $\|\mathbf{H}^+ \mathbf{Q}^{1/2}\|_{\text{F}}$ which, in general, is not a convex function of $\boldsymbol{\xi}$.

To solve this problem, we first propose a semi-analytic approach based on the Newton-Raphson method, outlined in Sec. V-A and, then, we propose a heuristic optimization algorithm, described in Sec. V-B.

A. Newton-Raphson SRE optimization

The optimal value for $\boldsymbol{\xi}$ solving (26), in the following denoted by $\boldsymbol{\xi}_{\text{opt}}$, is given by

$$\boldsymbol{\xi}_{\text{opt}} = \arg \min_{\boldsymbol{\xi} \in [0, 2\pi]^{2N+K}} \|\mathbf{H}^+ \mathbf{Q}^{1/2}\|_{\text{F}}^2 = \arg \min_{\boldsymbol{\xi} \in [0, 2\pi]^{2N+K}} \text{Tr} \{ (\mathbf{H}\mathbf{H}^{\text{H}})^{-1} \mathbf{Q} \}. \quad (27)$$

Note that \mathbf{H} is defined by (15), (16), (17), and (25). In particular \mathbf{H} depends on $\boldsymbol{\delta}$ only through matrix \mathbf{M} , on $\boldsymbol{\alpha}$ through matrices \mathbf{M} and \mathbf{T} , while it depends on $\boldsymbol{\psi}$ only through matrix $\boldsymbol{\Psi}$. Finally, matrices $\mathbf{V}^{(1)}$ and $\mathbf{V}^{(3)}$ are constant, given the geometry of the system. Let $f(\boldsymbol{\xi}) = \text{Tr} \{ (\mathbf{H}\mathbf{H}^{\text{H}})^{-1} \mathbf{Q} \}$. We can solve numerically (27) by the iterative Newton-Raphson method: given a starting point $\boldsymbol{\xi}^{(0)}$, the h -th estimate of $\boldsymbol{\xi}_{\text{opt}}$, $h = 1, 2, \dots$ is given by

$$\boldsymbol{\xi}^{(h)} = \boldsymbol{\xi}^{(h-1)} - \left[\boldsymbol{\mathcal{S}} \left(\boldsymbol{\xi}^{(h-1)} \right) \right]^{-1} \nabla f \left(\boldsymbol{\xi}^{(h-1)} \right), \quad (28)$$

where $\boldsymbol{\mathcal{S}} = \frac{\partial^2 f}{\partial \boldsymbol{\xi} \partial \boldsymbol{\xi}^{\text{T}}}$ is the Hessian matrix of $f(\boldsymbol{\xi})$. The expressions for ∇f and $\boldsymbol{\mathcal{S}}$ can be obtained in closed form. A detailed derivation is reported in Appendix B.

Iterations of the Newton-Raphson algorithm stop when the magnitude of the increment from one iteration to the next one falls below a predetermined threshold. Since $f(\boldsymbol{\xi})$ is not convex, several different starting points need to be taken, and the final approximation of $\boldsymbol{\xi}_{\text{opt}}$ is the (local) minimum point that yields the smallest value of $f(\boldsymbol{\xi})$.

B. Heuristic SRE optimization

Owing to the complexity of the optimization problem defined in (26), we propose a simpler heuristic approach to environment optimization. Specifically, we make the key observation that, if the IRS area is large enough, its radiation pattern is characterized by a narrow beam and, thus, will likely serve a single, properly chosen, UE. By restricting our attention to a solution where each UE is associated with one IRS and the IRSs–UEs channels are dominated by the LoS component, as reasonable in sub-THz/THz propagation, we are able to solve a substantially simpler problem, at a modest cost in terms of distance from (26), as shown in Section VII. Formally, this can be done by defining the map

$$\mathcal{M} : \{1, \dots, K\} \rightarrow \{1, \dots, N\}, \quad (29)$$

which associates UE k to IRS $\mathcal{M}(k)$. In practice, this means that IRS $\mathcal{M}(k)$ should be electronically rotated so as to point its beam in the direction of the UE k and, symmetrically, the UE k steers the beam generated by its ULA so that it points towards the IRS $\mathcal{M}(k)$. This criterion is particularly suited when the surfaces are sufficiently large and the UE ULAs have enough antennas so that the beam generated by IRS $\mathcal{M}(k)$ reaches UE k without interfering with other UEs.

So, under heuristic optimization and given the map \mathcal{M} , the electronic rotation angle of the IRS $\mathcal{M}(k)$ is set to

$$\delta_{\mathcal{M}(k)} = \frac{\phi_{\mathcal{M}(k)}^{(1)} - \phi_{k,\mathcal{M}(k),0}^{(2)}}{2}, \quad (30)$$

which yields $s_{k,\mathcal{M}(k),0} = 0$ in (25), and on the UE side the beam direction is set to $\alpha_k = \zeta_{k,\mathcal{M}(k)}$, so that $b_{k,\mathcal{M}(k),0} = 1$ in (18). Regarding phase shifts, we set the value of $\psi_{\mathcal{M}(k)}$ so that the signals reflected by the IRS and by the wall reach the UE with the same phase and, thus, generate constructive interference.

It is worth noting that, if $N > K$, there are $N - K$ IRSs which are not associated to any user. While in a scenario with small surfaces and single-antenna UEs, the contribution of these IRSs can be relevant, in the presence of narrow beams generated by the IRSs and high gain UE arrays, their effect is substantially negligible. If the n -th IRS is not associated to any UE, the heuristic algorithm conventionally set $\delta_n = 0$ and $\psi_n = 0$.

Let $\xi = \xi(\mathcal{M})$ be the value of ξ resulting from a given map \mathcal{M} . The proposed heuristic algorithm then consists in finding the optimal map, \mathcal{M}_{opt} , satisfying

$$\mathcal{M}_{\text{opt}} = \arg \min_{\mathcal{M}} \|\mathbf{H}_{\text{heu}}^+ \mathbf{Q}^{1/2}\|_{\text{F}}, \quad (31)$$

where \mathbf{H}_{heu} is the channel matrix obtained by setting $\xi = \xi(\mathcal{M})$ in the expression for \mathbf{H} in (15). Notice that, since there are $N!/(N - K)!$ possible maps, an exhaustive search of \mathcal{M}_{opt} is possible only for small-size scenarios.

VI. SENSITIVITY OF SRE OPTIMIZATION TO SYSTEM PARAMETERS

In this section, we analyze the sensitivity of SRE optimization, as described in the previous section, to some system parameters. In particular, we consider the impact on the received SNR in (23) of the size of the ULA arrays at the BS and at the UEs, and of the IRS areas. Moreover, in a properly defined limiting regime, we derive a simplified criterion for optimization.

A. Impact of the number of ULA array elements

We first notice that the number of elements of the BS ULA, M_1 , appears in matrix $\mathbf{V}^{(1)}$ whose n -th column is given by $\mathbf{v}_n^{(1)} = \mathbf{s}(\Delta_1, M_1, \beta_n^{(1)})$. Such matrix only depends on the geometry of the system and is not affected by electronic IRS rotation or phase shifts.

From (23), the received SNR depends on $\mathbf{V}^{(1)}$ through $\mathbf{V}^{(1)\text{H}}\mathbf{V}^{(1)}$, whose (n, n') entry is given by

$$\mathbf{v}_n^{(1)\text{H}}\mathbf{v}_{n'}^{(1)} = \frac{1}{M_1} \frac{\sin\left(2\pi\Delta_1 M_1 (\sin\beta_n^{(1)} - \sin\beta_{n'}^{(1)})\right)}{\sin\left(2\pi\Delta_1 (\sin\beta_n^{(1)} - \sin\beta_{n'}^{(1)})\right)}. \quad (32)$$

Now, for a given system geometry, the AoDs $\beta_1^{(1)}, \dots, \beta_n^{(1)}$ are fixed and we suppose that $\beta_n^{(1)} \neq \beta_{n'}^{(1)}$ for $n \neq n'$. Thus:

$$\left| \mathbf{v}_n^{(1)\text{H}} \mathbf{v}_{n'}^{(1)} \right| \leq \frac{1}{M_1 \left| \sin \left(2\pi \Delta_1 (\sin \beta_n^{(1)} - \sin \beta_{n'}^{(1)}) \right) \right|} \xrightarrow{M_1 \rightarrow \infty} 0 \quad (33)$$

for $n \neq n'$. This implies that $\lim_{M_1 \rightarrow \infty} \mathbf{V}^{(1)\text{H}} \mathbf{V}^{(1)} = \mathbf{I}_N$. Similarly, the parameter M_1 also appears in $\mathbf{V}^{(3)}$. Then, provided that $\beta_k^{(3)} \neq \beta_{k'}^{(3)}$ for $k \neq k'$, $\lim_{M_1 \rightarrow \infty} \mathbf{V}^{(3)\text{H}} \mathbf{V}^{(3)} = \mathbf{I}_K$. Finally, if $\beta_n^{(1)} \neq \beta_k^{(3)}$ for every pair of k and n , $\lim_{M_1 \rightarrow \infty} \mathbf{V}^{(1)\text{H}} \mathbf{V}^{(3)} = \mathbf{0}_{N \times K}$. As a consequence, when IRSs and UEs are angularly separated with respect to the BS,

$$\|\mathbf{H}^+ \mathbf{Q}^{1/2}\|_{\text{F}}^2 = \text{Tr} \{ (\mathbf{H}\mathbf{H}^{\text{H}})^{-1} \mathbf{Q} \} \xrightarrow{M_1 \rightarrow \infty} \text{Tr} \{ (\mathbf{M}\mathbf{M}^{\text{H}} + \mathbf{T}\mathbf{T}^{\text{H}})^{-1} \mathbf{Q} \}. \quad (34)$$

Notice that, in this asymptotic regime, the received SNR becomes independent of the phase shifts ψ . This happens because, when M_1 gets large, the columns of $\mathbf{V}^{(1)}$ become orthogonal and it is the precoder that allows to properly set the phases of the signals impinging to each IRS. Summarizing, we expect that *for increasing transmit array size, the impact of phase shifts, Ψ , on the received SNR decreases until it becomes negligible.*

B. Impact of IRS areas

As already observed, from the expression of $[\mathbf{M}]_{k,n}$ in (16) it can be seen that the width of the beam generated by the n -th IRS depends on its area, A_n . In particular, for $\frac{\sqrt{A_n}}{\lambda} \rightarrow \infty$:

$$[\mathbf{M}]_{k,n} \rightarrow c_n^{(1)} a_{k,n,p}^{(2)} c_{k,n,p}^{(2)} \sum_{p=0}^P b_{k,n,p} \delta[s_{k,n,p}], \quad (35)$$

where $\delta[x] = 1$ for $x = 0$ and $\delta[x] = 0$ otherwise. Thus, it turns out that the n -th IRS contributes to the signal received by the k -th UE only if it points towards one of the paths characterizing the IRS–UE channel. As a consequence, in the presence of a dominant LoS path we expect that *IRSs with large area (compared to λ^2) should be rotated so as to point in the direction of a given UE.*

C. SRE optimization algorithms in the asymptotic regime

In the doubly asymptotic regime $M_1, A_n \rightarrow \infty$, SRE optimization becomes easier to state and to solve. Indeed, thanks to (34), the optimization problem in (27) reduces to

$$\tilde{\boldsymbol{\xi}}_{\text{opt}} = \arg \min_{\tilde{\boldsymbol{\xi}} \in [0, 2\pi]^{N+K}} \text{Tr} \{ (\mathbf{M}\mathbf{M}^{\text{H}} + \mathbf{T}\mathbf{T}^{\text{H}})^{-1} \mathbf{Q} \}, \quad (36)$$

²The larger M_1 , the narrower the BS transmitted beam. Thus, for a too large value of M_1 , the hypothesis that the transmitted beam uniformly illuminates the IRSs does not hold. However, as we will see in Section VII, for a realistic scenario, this case does not happen.

where $\tilde{\boldsymbol{\xi}} = [\boldsymbol{\delta}, \boldsymbol{\alpha}]^T$. Moreover, if we suppose that UEs and multipath reflectors are angularly separated, as observed from the IRSs, then, by (35), we obtain that $[\mathbf{M}]_{k,n} \neq 0$ if and only if $n = \mathcal{M}(k)$. As a consequence, $\mathbf{M}\mathbf{M}^H$ becomes diagonal and the heuristic problem becomes

$$\mathcal{M}_{\text{opt}}^\infty = \arg \min_{\mathcal{M}} \omega(\mathcal{M}), \quad (37)$$

where

$$\omega(\mathcal{M}) = \sum_{k=1}^K \left(|[\mathbf{M}]_{k,\mathcal{M}(k)}|^2 + |[\mathbf{T}]_{k,k}|^2 \right)^{-1} q_k. \quad (38)$$

The above is an assignment problem whose weights are the sums of the squared magnitudes of the entries of \mathbf{M} and \mathbf{T} . The solution can be found by resorting to, e.g., the Hungarian algorithm [37]. It is important to highlight that the Hungarian algorithm has very low, namely, cubic complexity, hence, it can be efficiently used for realistically-sized problem instances.

We point out that, in a particular setup, the solution of (37), together with (14) is indeed the optimal choice for the phase shifts $\theta_{n,\ell,\ell'}$. To introduce the next proposition, we define μ_{kn} as the magnitude of the channel reaching user k through IRS n .

Proposition 2: Consider the system in (6), with $\tilde{\mathbf{H}}_k$ given by (9). Suppose $N = K = 2$, $P = 0$ (i.e., no multipath) and no wall reflection. Let the BS have full CSI and perform ZF precoding. Finally, we concentrate on the asymptotic scenario in which $M_1 \rightarrow \infty$ and $L_n \rightarrow \infty$. Under these hypotheses, if $\mu_{11} > \mu_{21}$ and $\mu_{22} > \mu_{12}$, or, conversely, $\mu_{11} < \mu_{21}$ and $\mu_{22} < \mu_{12}$, the solution of (37) (with the phase shifts in (14)) is optimal in the sense that it minimizes $\|\tilde{\mathbf{H}}^+\|_{\text{F}}^2$ (see (26)).

Proof: See Appendix C. ■

In the next section, we will show when, in a realistic scenario, conditions for the asymptotic regime are met. In such conditions, the heuristic algorithm in its simplified version (37)-(38) represents a feasible way of SRE optimization. We observe that the ZF precoder $\boldsymbol{\Gamma}$ tends to be a simple equalizing beamformer in the asymptotic regime, since the channels corresponding to the K users become orthogonal by themselves, and $\boldsymbol{\Gamma}$ tends to split the power among the different channels in order to meet the relative quality of service dictated by matrix \mathbf{Q} .

VII. PERFORMANCE COMPARISON OF THE PROPOSED OPTIMIZATION ALGORITHMS

We now assess the performance of the optimization algorithms proposed in Section V and show the influence of the system parameters on the SNR and on the achievable rate at the UEs. To this purpose we consider the test scenario in Fig. 3, depicting an area of 100 m², whose vertices, are the points (0, 0), (10, 0), (0, 10) and (10, 10) (all coordinates expressed in meters). The BS is located at (0, 5) and the N IRSs, denoted by the labels IRS1, ...,

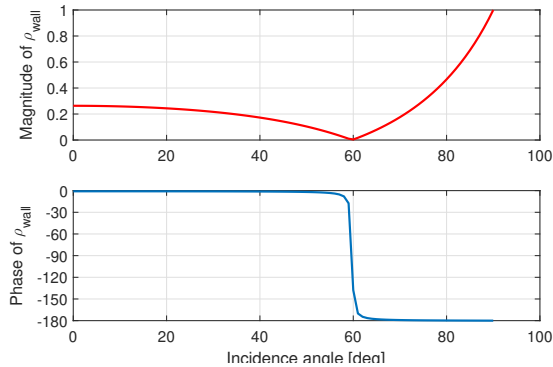


Fig. 2. Amplitude (above) and phase (below) of the complex reflection coefficient ρ_{wall} , for plasterboard panels, plotted versus the AoA of the BS signal. The incidence angle is measured from the direction orthogonal to the wall.

IRS N , have area $A_n = A$ and are equally spaced along a wall coinciding with the x axis. The positions of the K UEs, denoted by the labels UE1, ..., UE K , are random variables, uniformly distributed in the rectangle \mathcal{U} whose vertices are $(2.5, 4)$, $(10, 4)$, $(10, 10)$ and $(2.5, 10)$.

The signal transmitted by the BS has bandwidth $B = 100$ MHz and carrier frequency $f_0 = 0.1$ THz, corresponding to the wavelength $\lambda = 3$ mm. At such frequency the attenuation due to molecular absorption is negligible [28]; we therefore set $\kappa = 0$ in (8). The BS transmit power is $\mathcal{P}_t = 1$ W and we set $\mathbf{Q} = \mathbf{I}$, i.e., all users have the same received SNR. Finally, the separation of the elements of the BS and UE ULAs is set to $\Delta_1 = \Delta_2 = \lambda/2$.

The noise power at the receivers is set to $\sigma^2 = N_0 B$ where $N_0 = -174$ dBm/Hz. We also assume ideal reflection at the IRSs, i.e., $\rho_{\text{IRS}} = 1$. The wall acting as reflector for the BS signal coincides with the x axis depicted in Fig. 3. We assume it is made of plasterboard whose reflection coefficient, ρ_{wall} , is plotted in Figure 2 versus the AoA of the BS signal. The IRS-UE channels are random and affected by multipath and log-normal shadowing. Unless otherwise stated, we assume full knowledge of the channel state at the BS.

We evaluate the performance of the following techniques to solve the problem in (26):

- the joint optimization of the IRS electronic rotation angles, δ , of the phase shifts, ψ , and of the UE beam directions, α , by employing the Newton-Raphson algorithm, in the following referred to as “NRP”;
- the joint optimization of the IRS electronic rotation angles and of the UE beam directions by employing the Newton-Raphson algorithm, while setting to zero the IRS phase shifts. This technique, denoted as “NR”, solves (26) by imposing $\psi = \mathbf{0}$;
- the heuristic optimization algorithm, “HOP” described in Section V-B and based on the

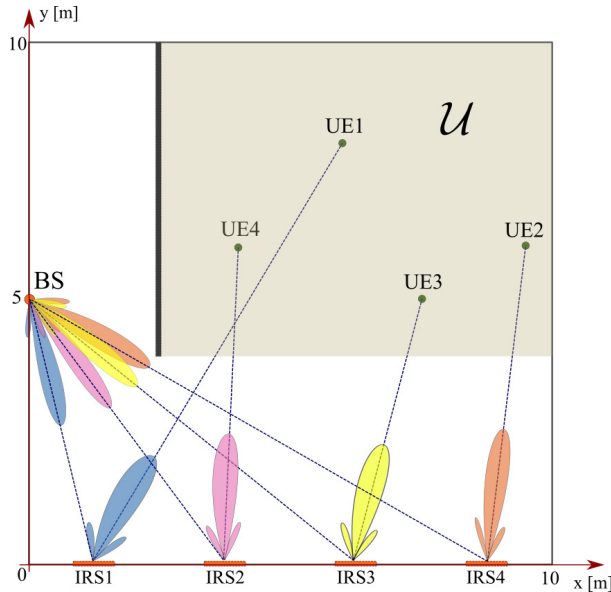


Fig. 3. An example of the system geometry considered in Section VII for $N = K = 4$. The IRSs are equally spaced, and the UE are uniformly distributed in the area \mathcal{U} . The plasterboard reflecting wall coincides with the x axis.

evaluation of (37)-(38). This algorithm takes the phase shifts, ψ , into account for the optimization.

Since, in general, the expression of the SNR in (23) is not convex in ξ , for each instance of the system geometry and of the channel, we perform $U = 100$ runs of the “NR” and “NRP” algorithms, each characterized by a different, randomly generated, starting point $\xi_u^{(0)}$, $u = 1, \dots, U$ and an output SNR_u . Then, for each realization of the UE positions, the SNR provided by the algorithms is given by $\max_u \text{SNR}_u$.

The numerical results are organized as follows: in Section VII-A, we show examples of the radiation patterns emitted by the IRSs and by the BS ULA, while in Section VII-B we compare the performance of the above optimization techniques in terms of the achieved SNR. Finally, in Section VII-C, we evaluate the impact of the system parameters on the network throughput.

A. Radiation patterns

We first describe the system behavior in a simple case where we neglect (i) shadowing effects, (ii) the reflection due to the plasterboard wall, and (iii) the existence of NLoS paths in the IRS-UE links. We also consider a BS ULA with $M_1 = 32$ elements, $N = 4$ IRSs of area $A = 100 \text{ cm}^2$ and $K = 4$ UEs equipped with a single isotropic antenna ($M_2 = 1$), whose positions are shown in Fig 3. The “HOP” algorithm applied to this scenario selects the IRS-UE assignment depicted in Fig. 3 by solid lines. Specifically, the IRSs 1,2,3, and 4

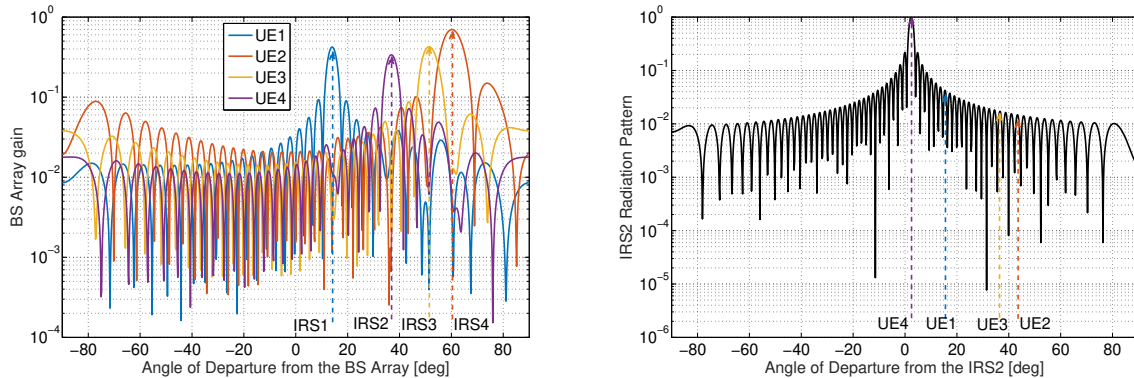


Fig. 4. (Left) BS array gains $|G_k|^2$, for each of the $K = 4$ data streams in the scenario depicted in Fig. 3. The dashed arrows indicate the directions of the IRSs as observed from the BS. (Right) Radiation pattern of IRS2, whose size is $A = 100 \text{ cm}^2$, for the IRS-UE assignment as shown in Fig. 3. The dashed lines indicate the directions of the users as observed by the IRS.

are electronically rotated so as to point their beams, respectively, towards UEs 1,4,3, and 2. Referring to (29), this assignment corresponds to the map $\mathcal{M}(1) = 1$, $\mathcal{M}(2) = 4$, $\mathcal{M}(3) = 3$, and $\mathcal{M}(4) = 2$.

The BS, thanks to the precoder Γ , generates K beams, one for each UE. The radiation pattern of the k -th beam as a function of the AoD from the BS ULA, denoted by β , is given by $G_k = \mathbf{s}(\Delta_1, M_1, \beta)^H \boldsymbol{\gamma}_k$, $k = 1, \dots, K$, where $\boldsymbol{\gamma}_k$ is the k -th columns of the precoder Γ . To get insight on how the signal energy is distributed among the IRSs, in Fig. 4(left) we show the array gains $|G_k|^2$, $k = 1, \dots, 4$ plotted versus β . As can be observed, the radiation pattern for the data stream intended for UE1 (blue line) clearly shows a main lobe in the direction of the IRS1 since such surface steers the signal towards UE1. Similarly, the radiation patterns for UE2, UE3 and UE4 show peak values in the direction of their associated IRS4, IRS3 and IRS2, respectively. However, note that a fraction of the signal energy intended for UE1 is also sent to IRSs other than IRS1, due to side lobes of the radiation pattern. Similarly, side lobes in the IRS radiation pattern may generate interference at the UEs as shown by Fig. 4(right), which reports the radiation pattern of IRS2. In the figure, the dashed lines indicate the directions of the users as observed by IRS2. As can be seen, although the main lobe is directed towards UE4, a side lobe points towards UE1, albeit with a 15-dB lower gain. However, the resulting interference at the UEs is canceled out by a proper setting of the IRSs phase shifts. Thus, the overall user channels are orthogonal, as granted by the ZF filter. Fig. 4(right) also shows that the IRS behaves as an ‘‘anomalous’’ reflector. Indeed, the AoA of the BS signal at IRS2 is 36.8° while the reflected beam has an AoD of 2.4° . As

mentioned in Section III, the area of an IRS affects the beamwidth of its radiation pattern. For an IRS area of 100 cm^2 , the first-null beamwidth is about 2° . We point out that the radiation pattern in Fig. 4(right) has been obtained by assuming an ideal IRS reflection coefficient, $\rho_{\text{IRS}} = 1$. However, if ρ_{IRS} is phase-shift dependent [30] the radiation pattern might differ from that depicted in the figure; in particular it could show a lower gain of the main lobe and higher side lobes. Furthermore, if the system allows to control the amplitude response of each meta-atom, the radiation pattern can be designed e.g. to minimize the side lobes power at a price of a slight increase of the main lobe beamwidth.

B. Effect of the plasterboard wall

We now investigate the performance of the “NR” “NRP” and “HOP” optimization algorithms and the impact of the system parameters on the received SNR.

First of all, we measure the effect of the signal reflected by the plasterboard wall. In Fig. 5(left) we therefore consider a single-user scenario ($K = 1$), a single IRS ($N = 1$), no multipath on the IRS-UE link ($P = 0$), no shadowing, and $M_1 = 4$ and $M_2 = 1$ antenna elements at the BS and UE, respectively. The optimization here consists only in the proper choice of the electronic rotation δ_1 of the IRS1 and of the phase shift ψ_1 , since for $M_2 = 1$ the UE antenna is isotropic and there is no beam direction to be optimized. Clearly, the choice of δ_1 is trivial, since the optimum is achieved when the beam generated by the IRS points towards the UE; in such a case “NRP”, and “HOP” are expected to provide the same performance. Then, given the UE position, we choose δ_1 so as to null $s_{1,1,0}$ in (25). Moreover, in presence of the wall reflection, the IRS phase shift ψ_1 should be set so as to ensure constructive interference at the UE. The cumulative density function (cdf) of the SNR at the UE, obtained by generating 1000 realizations of the above described scenario, is reported in Fig. 5(left) for IRSs of area $A = 1 \text{ cm}^2$ and $A = 100 \text{ cm}^2$. For $A = 1 \text{ cm}^2$ the SNR is dominated by the contribution of the signal reflected by the wall, which yields a gain of about 25 dB with respect to the scenario without wall reflection. Instead, for $A = 100 \text{ cm}^2$, the beneficial contribution of the wall is limited to about 1.5 dB. This means that IRS areas should be accurately designed depending on the number and quality of natural reflectors in the environment. IRS with small area provide little contribution to the received power while larger IRS allow to neglect the contribution due to natural reflectors. We also note that, in the absence of wall reflection, by increasing the IRS area from 1 cm^2 to 100 cm^2 we obtain 40 dB improvement in the SNR. This is expected since, from (16) and as observed in [35], the SNR depends on A^2 .

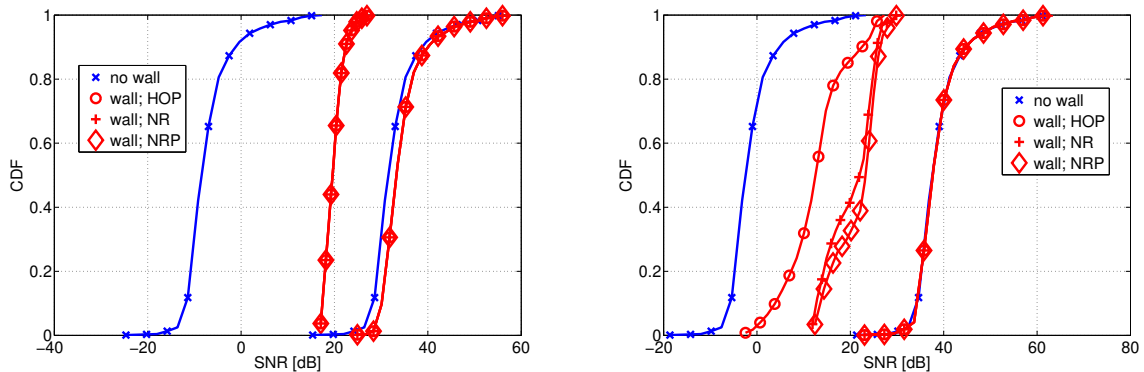


Fig. 5. Cdf of the SNR for $N = K = 1$, $M_1 = 4$, $M_2 = 1$ (left) or $M_2 = 4$ (right) and IRS area $A = [1, 100] \text{ cm}^2$, in the presence or absence of the reflection due to the plasterboard wall. The channels are considered singlepath and not affected by shadowing.

In Fig. 5(right), we consider the same setting as in Fig. 5(left) but $M_2 = 4$ elements. In this case, the received SNR also depends on the direction, α_1 , of the beam generated by the UE ULA and, therefore, the SNR optimization in (26) is not as trivial as before, and the “NR”, “NRP”, and “HOP” algorithms provide different performance. Specifically, while all algorithms agree that the IRS should point its beam towards the UE, they return divergent choices for the angle α_1 . In particular,

- the “NRP” algorithm rotates the UE beam so as to maximize the received energy at the UE. The optimal direction is, in general, in between the directions of the beams reflected by the IRS and by the wall. Also, “NRP” adjusts the IRS phase shift, so as to create constructive interference of the two signals at the UE;
- “NR” operates similarly to “NRP”, but it does not optimize the phase shift ψ_1 ;
- “HOP” points the UE beam towards the IRS, thus neglecting the effect of the wall.

Significant performance gaps arise when the IRS area is small. For $A = 1 \text{ cm}^2$, the “HOP” algorithm performs poorly since it points the UE beam towards the IRS, which provides a very weak signal compared to that reflected by the wall. Instead, “NRP” and “NR” perform similarly, since they both steer the UE beam towards the stronger energy source. However “NRP” performs 1–4 dB better than “NR” since the latter does not optimize the phase ψ_1 . Instead, for $A = 100 \text{ cm}^2$, “HOP” performs identically to the much more complex “NRP” and “NR”. We also observe that, for $A = 100 \text{ cm}^2$, the curves in Fig. 5(right) show a 6 dB gap w.r.t. those shown in Fig. 5(left), due to the gain of the UE ULA with respect to an isotropic antenna. We conclude that IRSs with area as large as 100 cm^2 are required, in order to collect and reflect enough signal energy to dominate the effect of natural reflectors such

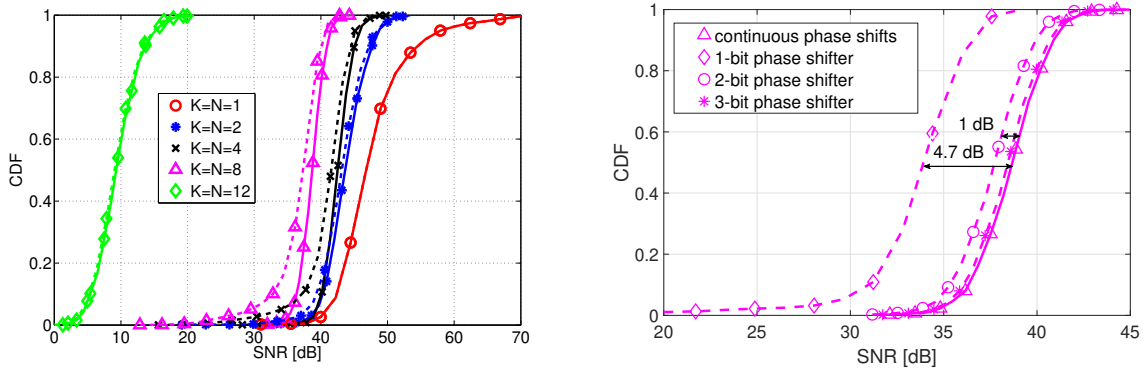


Fig. 6. Cdf of the SNR provided by “HOP” for $M_1 = 32$, $M_2 = 4$, $A = 100 \text{ cm}^2$, in the presence of multipath and shadowing. (Left) $N = K = [1, 2, 4, 8, 12]$ assuming continuous phase shifters, (right) $N = K = 8$ assuming b -bit phase shifters.

as the plasterboard wall. On the base of this consideration, in the following we will neglect the contribution of the signal reflected by the plasterboard wall.

C. Impact of the system parameters on the network performance

Here we investigate the impact of IRS and UE number on network performance when shadowing effects and unwanted obstacles are present. In Fig. 6 (left) we consider a multi-user scenario and measure the cdf of the SNR for the case $M_1 = 32$, $M_2 = 4$, $A = 100 \text{ cm}^2$, $N = K$, and $K = [1, 2, 4, 8, 12]$. The results refer to the “HOP” algorithm, since “NR” and “NRP” do not provide significant performance improvements w.r.t. “HOP”.

The links from BS to IRSs are assumed to be LoS, whereas the IRS–UE channels follow the model in (11) where $P = 2$ NLoS path are considered. Each NLoS path is characterized by a reflector randomly positioned in the area \mathcal{U} and characterized by a reflection coefficient $|\rho_{k,n,p}|^2 = -10 \text{ dB}$. All the links experience shadowing effects, i.e., the r.v. $\alpha_{k,n,p}^{(2)}$ are log-normal distributed with variance $\sigma_{\text{sh}} = 2 \text{ dB}$. We also neglect the reflection due to the plasterboard wall. For each value of K two curves are reported. The solid line refers to the case where the BS has full knowledge of the channel state, including the shadowing coefficients, the position of the reflectors and of the users; the dashed line refers to the case where the BS knowledge is limited to the LoS paths of each IRS-UE channel, i.e., it assumes $P = 0$ and has knowledge of the UEs positions and of the shadowing coefficients $a_{k,n,0}$. In the latter case the BS is unable to apply the proper ZF filter and, thus to grant an interference free channel to the UEs. This clearly entails a performance loss which, however, is negligible for $K = 1, 2$, and amounts to about 1 dB and 2 dB for $K = 4$ and $K = 8$, respectively.

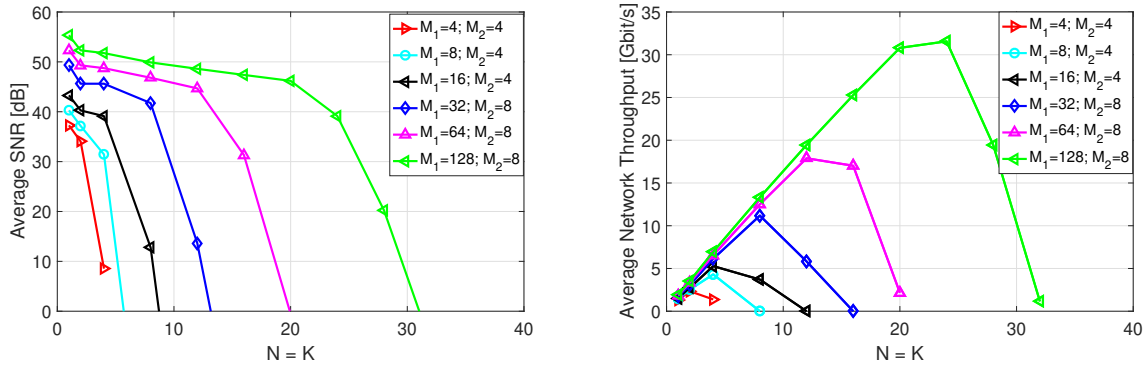


Fig. 7. Average SNR [dB] (Left) and average network throughput R [Gbit/s] (Right) versus the number of users, $K = N$, as M_1 and M_2 vary. The IRSs' area is $A = 100 \text{ cm}^2$.

Since the total transmitted power \mathcal{P}_t is evenly shared among users, we expect a 3-dB SNR loss as K doubles. In the figure this can be observed up to a certain value of K . However, as K grows, the SNR loss becomes larger, i.e., it increases to 5 dB when moving from $K = 4$ to $K = 8$, and is as high as 22 dB when increasing K from 8 to 12. This behavior can be explained as follows. As K and N increase, the distance between adjacent IRSs becomes smaller and so does the average distance among UEs. When adjacent IRSs are very close to each other, the BS beam associated to a given UE is not narrow enough to illuminate a single IRS. Similarly, the beams reflected by the IRSs are not narrow enough to illuminate a single UE. In other words, as K increases, many channels become “almost” linearly dependent, making the channel matrix ill conditioned, with many eigenvalues close to 0. Then, the pseudoinverse \mathbf{H}^+ in (23) shows large eigenvalues which have a detrimental effect on the SNR. In this situation already compromised, imperfect knowledge of the channel at the BS has negligible impact, i.e. for $K = 12$ the solid and dashed lines are superimposed.

For the same system setting, Fig. 6 (right) shows the performance degradation incurred when b -bit discrete phase shifters are employed. The SNR losses measured when $N = K = 8$ and $b = 1, 2, 3$ are respectively 4.7 dB, 1 dB and 0.2 dB and are consistent with the values reported in [34, Table I] for an asymptotic (large- L_n) regime, i.e. 3.9 dB, 0.9 dB and 0.2 dB. The effect of user densification is further investigated in Fig. 7(left) which shows the average SNR plotted versus K , for different values of M_1 and M_2 in the same setting of Fig. 6, where the BS has full knowledge of the channel state.

The curves show an interesting behavior: for small K the SNR slowly decreases as K increases, with a 3 dB loss as K doubles; instead, for large values of K , we observe a significant performance drop. Again, this is explained by observing that for large K the

BS beams are not narrow enough to illuminate a single IRSs, i.e., adjacent IRS cannot be “separated” by the BS ULA. Hence the BS-UE channels cannot be easily orthogonalized.

The overall system performance can also be measured in terms of the average network throughput, defined as $T = K \cdot B \cdot \mathbb{E}[R]$, where B is the signal bandwidth and R is the spectral efficiency in (24). Fig. 7(right) shows the average network throughput as a function of the number of supported users, for different values of M_1 and M_2 . For each pair (M_1, M_2) , the throughput initially increases with K . In such a situation the system load is moderate and the network is able to accommodate more and more UEs. For $K = K^*$ the system reaches saturation and the throughput starts falling. For example, for $M_1 = 128$ and $M_2 = 8$, we have $K^* = 20$ and about 32 Gbit/s can be achieved. Also, we observe that by doubling M_1 we can double the maximum network throughput. Indeed, as M_1 increases, the beamwidth of the BS beams decreases and more IRS can be separated and supported.

As a conclusion, the number of UEs, K^* , corresponding to the peak network throughput can be seen as the maximum order of space division multiplexing that the IRSs can provide in the particular scenario investigated. For such number of UEs, in fact, we serve as many users as possible without compromising the performance, because of the essentially interference-free channels established from the BS to the users. For this IRS-assisted environment, the space-division multiple-access ability of the system is increased by increasing the size of the arrays at the BS and the UEs, for a sufficiently large area of the meta-surfaces.

VIII. CONCLUSIONS

In this work we tackle the optimization of a SRE composed of a multiuser wireless network operating in the sub-THz/THz frequency bands and of a set of IRSs. IRS are employed to improve the BS-UEs channels when direct BS-UEs LoS links are unavailable. We considered a channel model able to capture the main characteristics of sub-THz/THz propagation such as molecular absorption, multipath, the presence of large solid objects acting as reflectors, and large-scale fading effects.

Motivated by the extreme sparsity of the sub-THz/THz channel, by the high gain provided by the transmit and receive antenna arrays, and by the aim of providing simple solutions for a practical SRE implementation, we modeled the behavior of each IRS through only two parameters, namely, the phase-gradient and the phase-shift, abstracting its size and individual components. According to this model IRSs behave as electronically steerable reflectors, obeying the generalized Snell law.

We have shown that such choice, although suboptimal in a general multiuser scenario, is indeed optimal in many practical relevant cases. Furthermore, it is extremely appealing since it allows to significantly reduce the complexity of SRE optimization. Such task is further facilitated by the adoption, at the BS, of a ZF precoder which orthogonalize UEs channels and allows to apply a semi-analytic approach to the optimization algorithms. We also provided a set of asymptotic results which provide insight on the system behavior when the IRSs have large area and the number of antenna elements at the BS grows large.

Capitalizing on this network model, we have proposed a simple manageable formulation of the SRE optimization problem, which aim at maximizing the SNR measured at the UE, whereas the optimization variables are the electronic rotations and the phase shifts of the IRSs, as well as the direction of the beams generated by the UE ULAs. To solve the problem we proposed an algorithm based on Newton-Raphson method and a simple heuristic approach based on the Hungarian algorithm and on a map associating UEs with IRSs.

Our numerical results provide multiple valuable insight. First, if surfaces are large enough (e.g. 100 cm² in our setup), the influence of large static reflectors (as walls) can be neglected. Second, with a sufficiently large number of antennas at the BS, the heuristic algorithm performs similarly to the more complex Newton-Raphson approach. Third, as a general rule the number of users supported by the system depends on the number of antennas at the BS. Finally, the SNR degradation incurred when discrete phase shifters are employed is consistent to that obtained in an asymptotic (large- L_n) regime. We observe, however, that geometry also plays an important role since the system performance show a dramatic drop when the IRS density is so high that they cannot be angularly separated at the UEs.

In addition to being interesting in themselves, such results further the high level goal of designing and implementing practical, simple and efficient IRS aided communication systems working in the THz frequency bands.

APPENDIX A

PROOF OF PROPOSITION 1

By using the definitions of the matrices $\mathbf{H}_n^{(1)}$, $\bar{\Theta}_n$, $\mathbf{H}_{k,n}^{(2)}$, and $\mathbf{H}_n^{(3)}$, the vector $\mathbf{f}_k^H \tilde{\mathbf{H}}_k$ appearing in (5) can be rewritten as

$$\begin{aligned} \mathbf{f}_k^H \tilde{\mathbf{H}}_k &= \sum_{n=1}^N \sum_{p=0}^P \frac{t_{k,n,p}}{L_n} \left(\mathbf{1}_{L_n}^T \otimes \mathbf{u}_{k,n,p}^{(2)} \right)^H \left(\mathbf{I}_{L_n} \otimes \bar{\Theta}_n \right) \left(\mathbf{1}_{L_n} \otimes \mathbf{u}_n^{(1)} \right) \mathbf{v}_n^{(1)H} + \mathbf{f}_k^H \mathbf{H}_k^{(3)} \\ &= \sum_{n=1}^N \sum_{p=0}^P t_{k,n,p} \left(\mathbf{u}_{k,n,p}^{(2)H} \bar{\Theta}_n \mathbf{u}_n^{(1)} \right) \mathbf{v}_n^{(1)H} + t_k \mathbf{v}_k^{(3)H}, \end{aligned} \quad (39)$$

where $t_{k,n,p} \triangleq b_{k,n,p} \rho_n c_n^{(1)} c_{k,n,p}^{(2)}$, $t_k \triangleq b_k \rho^{\text{wall}} c_k^{(3)}$, $b_{k,n,p} \triangleq \mathbf{f}_k^H \mathbf{w}_{k,n,p}^{(2)}$, and $b_k \triangleq \mathbf{f}_k^H \mathbf{w}_k^{(3)}$. Furthermore, by recalling the definitions of $\mathbf{u}_n^{(1)}$, $\mathbf{u}_{k,n,p}^{(2)}$ and Θ_n , and by assuming uniform illumination of the meta-surface we get

$$\begin{aligned} \mathbf{u}_{k,n,p}^{(2)H} \Theta_n \mathbf{u}_n^{(1)} &= \frac{e^{j\psi_n}}{L_n} e^{j\pi\Delta(L_n-1)s_{k,n,p}} \sum_{\ell=1}^{L_n} e^{-j2\pi\Delta(\ell-1)s_{k,n,p}} \\ &= e^{j\psi_n} \frac{\text{sinc}(\Delta L_n s_{k,n,p})}{\text{sinc}(\Delta s_{k,n,p})}, \end{aligned} \quad (40)$$

where $s_{k,n,p} = \sin \phi_n^{(1)} - \sin \phi_{k,n,p}^{(2)} - g_n$. Then,

$$\mathbf{f}_k^H \tilde{\mathbf{H}}_k = \sum_{n=1}^N \sum_{p=0}^P t_{k,n,p} e^{j\psi_n} \frac{\text{sinc}(\Delta L_n s_{k,n,p})}{\text{sinc}(\Delta s_{k,n,p})} \mathbf{v}_n^{(1)H} + t_k \mathbf{v}_k^{(3)H}. \quad (41)$$

Now, as L_n increases, while the area A_n remains constant, we have $\lim_{L_n \rightarrow \infty} \text{sinc}\left(\sqrt{\frac{A_n}{L_n^2 \lambda^2}} s_{k,n,p}\right) =$

1. It follows that $\lim_{L_n \rightarrow \infty} \mathbf{f}_k^H \tilde{\mathbf{H}}_k = \sum_{n=1}^N \sum_{p=0}^P t_{k,n,p} \text{sinc}\left(\sqrt{\frac{A_n}{\lambda^2}} s_{k,n,p}\right) e^{j\psi_n} \mathbf{v}_n^{(1)H} + t_k \mathbf{v}_k^{(3)H}$.

Since the vector $\mathbf{f}_k^H \tilde{\mathbf{H}}_k$ is the k -th row of the matrix $\tilde{\mathbf{H}}$ we can write

$$\mathbf{H} = \lim_{L_1, \dots, L_N \rightarrow \infty} \tilde{\mathbf{H}} = \mathbf{M} \Psi \mathbf{V}^{(1)H} + \mathbf{T} \mathbf{V}^{(3)H}, \quad (42)$$

$[\mathbf{M}]_{k,n} = \rho_n c_n^{(1)} \sum_{p=0}^P b_{k,n,p} c_{k,n,p}^{(2)} \text{sinc}\left(\sqrt{\frac{A_n}{\lambda^2}} s_{k,n,p}\right)$, $\Psi = \text{diag}(e^{j\psi_1}, \dots, e^{j\psi_N})$, $\mathbf{V}^{(1)} = [\mathbf{v}_1^{(1)}, \dots, \mathbf{v}_N^{(1)}]$, $\mathbf{V}^{(3)} = [\mathbf{v}_1^{(3)}, \dots, \mathbf{v}_K^{(3)}]$, and $\mathbf{T} = \text{diag}(t_1, \dots, t_K)$. Finally, by recalling the expressions for \mathbf{f}_k , $\mathbf{w}_{k,n,p}^{(2)}$ and $\mathbf{w}_k^{(3)}$ we obtain

$$b_{k,n,p} \triangleq \frac{\text{sinc}(\Delta_2 M_2 (\sin \alpha_k - \sin \zeta_{k,n,p}))}{\text{sinc}(\Delta_2 (\sin \alpha_k - \sin \zeta_{k,n,p}))}; \quad b_k \triangleq \frac{\text{sinc}(\Delta_2 M_2 (\sin \alpha_k - \sin \zeta_k))}{\text{sinc}(\Delta_2 (\sin \alpha_k - \sin \zeta_k))}. \quad (43)$$

APPENDIX B

DERIVATION OF ∇f AND \mathcal{S}

We are interested in computing the gradient and the Hessian of the term $\|\mathbf{H}^+ \mathbf{Q}^{1/2}\|_{\text{F}}^2$ appearing in (23) where $\mathbf{H} = \mathbf{M} \Psi \mathbf{V}^{(1)H} + \mathbf{T} \mathbf{V}^{(3)H}$. First of all, we define $\mathbf{K} = \mathbf{H} \mathbf{H}^H$ and we observe that $\|\mathbf{H}^+ \mathbf{Q}^{1/2}\|_{\text{F}}^2 = \text{Tr}\{\mathbf{K}^{-1} \mathbf{Q}\}$. Let $\boldsymbol{\delta} = [\delta_1, \dots, \delta_N]^T$, $\boldsymbol{\psi} = [\psi_1, \dots, \psi_N]^T$, and $\boldsymbol{\alpha} = [\alpha_1, \dots, \alpha_K]^T$, be the vectors of variables to be optimized. Then we can define $f(\boldsymbol{\delta}, \boldsymbol{\psi}, \boldsymbol{\alpha}) \triangleq \text{Tr}\{\mathbf{K}^{-1} \mathbf{Q}\}$. Let x be a generic argument of the function $f(\cdot)$, and let \mathbf{A} be a matrix. Then we define $\frac{\partial \mathbf{A}}{\partial x} = \mathbf{A}_{(x)}$. Also, the first derivative of $f(\cdot)$ w.r.t. x is given by

$$\begin{aligned} \frac{\partial f}{\partial x} &= \sum_{i,j} \frac{\partial \text{Tr}\{\mathbf{K}^{-1} \mathbf{Q}\}}{\partial K_{i,j}} \frac{\partial K_{i,j}}{\partial x} = \sum_{i,j} \text{Tr} \left\{ \frac{\partial \text{Tr}\{\mathbf{Y}^{-1} \mathbf{Q}\}}{\partial \mathbf{Y}} \bigg|_{\mathbf{Y}=\mathbf{K}} \frac{\partial \mathbf{K}}{\partial K_{i,j}} \right\} \frac{\partial K_{i,j}}{\partial x} \\ &= - \sum_{i,j} \text{Tr} \left\{ (\mathbf{K}^{-1} \mathbf{Q} \mathbf{K}^{-1})^T \mathbf{J}^{(i,j)} \right\} \frac{\partial K_{i,j}}{\partial x}, \end{aligned} \quad (44)$$

where the last equality comes from [38, Eq. (121)]. In (44), \mathbf{Y} is a matrix whose entries are independent variables, and $\mathbf{J}^{(i,j)} = \frac{\partial \mathbf{K}}{\partial K_{i,j}}$ represents the structure of the matrix \mathbf{K} . The matrix

\mathbf{K} is complex Hermitian, thus $[\mathbf{J}^{(i,j)}]_{m,n} = 0$ for $(m,n) \neq (i,j)$ and $(m,n) \neq (j,i)$. Clearly $[\mathbf{J}^{(i,j)}]_{i,j} = 1$, whereas³ $[\mathbf{J}^{(i,j)}]_{j,i} = \frac{\partial K_{j,i}}{\partial K_{i,j}} = \frac{\partial K_{i,j}^*}{\partial K_{i,j}} = 0$. Then, from (44) we obtain

$$\frac{\partial f}{\partial x} = - \sum_{i,j} [\mathbf{K}^{-1} \mathbf{Q} \mathbf{K}^{-1}]_{j,i} \frac{\partial K_{i,j}}{\partial x} = - \text{Tr} \left\{ \mathbf{K}^{-1} \mathbf{Q} \mathbf{K}^{-1} \frac{\partial \mathbf{K}}{\partial x} \right\} = - \text{Tr} \{ \mathbf{Z} \mathbf{K}_{(x)} \},$$

where $\mathbf{Z} \triangleq \mathbf{K}^{-1} \mathbf{Q} \mathbf{K}^{-1}$. Now let y be another argument of the function $f(\boldsymbol{\delta}, \boldsymbol{\psi}, \boldsymbol{\varphi})$. The second mixed derivative of $f(\cdot)$ is given by

$$\frac{\partial^2 f}{\partial x \partial y} = - \frac{\partial}{\partial y} \text{Tr} \{ \mathbf{Z} \mathbf{K}_{(x)} \} = - \text{Tr} \left\{ \frac{\partial \mathbf{Z}}{\partial y} \mathbf{K}_{(x)} + \mathbf{Z} \frac{\partial}{\partial y} \mathbf{K}_{(x)} \right\}. \quad (45)$$

Now observe that $\frac{\partial \mathbf{Z}}{\partial y} = -2\mathbf{Z} \mathbf{K}_{(y)} \mathbf{K}^{-1}$. Thus we obtain

$$\frac{\partial^2 f}{\partial x \partial y} = - \text{Tr} \{ -2\mathbf{Z} \mathbf{K}_{(y)} \mathbf{K}^{-1} \mathbf{K}_{(x)} + \mathbf{Z} \mathbf{K}_{(xy)} \} = \text{Tr} \{ \mathbf{Z} (2\mathbf{K}_{(y)} \mathbf{K}^{-1} \mathbf{K}_{(x)} - \mathbf{K}_{(xy)}) \} \quad (46)$$

where $\mathbf{K}_{(xy)} = \frac{\partial}{\partial y} \mathbf{K}_{(x)}$. The Hessian of $f(\cdot)$ is then defined in terms of the derivatives of \mathbf{K}

$$\mathbf{K}_{(x)} = \frac{\partial}{\partial x} \mathbf{H} \mathbf{H}^H = \mathbf{H}_{(x)} \mathbf{H}^H + \mathbf{H} \mathbf{H}_{(x)}^H, \quad (47)$$

and, thus $\mathbf{K}_{(xy)} = \mathbf{H}_{(xy)} \mathbf{H}^H + \mathbf{H}_{(x)} \mathbf{H}_{(y)}^H + \mathbf{H} \mathbf{H}_{(xy)}^H + \mathbf{H}_{(y)} \mathbf{H}_{(x)}^H$. The derivatives of \mathbf{H} are easy to obtain from (15). In particular the matrix \mathbf{M} depends on both $\boldsymbol{\delta}$ and on $\boldsymbol{\alpha}$, the matrix $\boldsymbol{\Psi}$ depends on $\boldsymbol{\psi}$ only, and \mathbf{T} depends on $\boldsymbol{\alpha}$ only. The obtained expressions are quite cumbersome and, for simplicity, are not reported here.

APPENDIX C

PROOF OF PROPOSITION 2

We start from (39) and we specialize it to the case $K = N = 2$, $P = 0$ and no wall reflection (i.e., $t_k = 0$ for all k). We can write the overall channel matrix from the BS to the 2 UEs as $\tilde{\mathbf{H}} = \tilde{\mathbf{M}} \mathbf{V}^{(1)H}$, with $\mathbf{V}^{(1)}$ defined as in Prop. 1, and $\tilde{\mathbf{M}}$ a 2×2 matrix, with (k,n) element $\tilde{m}_{k,n} = t_{k,n} \mathbf{u}_{k,n}^{(2)H} \boldsymbol{\Theta}_n \mathbf{u}_n^{(1)} = t_{k,n} \mathbf{u}_{k,n}^{(2)H} \tilde{\mathbf{u}}_n$ where we have dropped the subscript p and we have defined the length- L_n norm-1 vector $\tilde{\mathbf{u}}_n$, which satisfies the equimodular property $|(\tilde{\mathbf{u}}_n)_i| = 1/\sqrt{L_n}$. We define the optimal value of the IRS phase shifts as the one that minimizes $\|\tilde{\mathbf{H}}^+ \mathbf{Q}^{1/2}\|_{\text{F}}^2$, where $\tilde{\mathbf{H}}^+ = \tilde{\mathbf{H}}^H (\tilde{\mathbf{H}} \tilde{\mathbf{H}}^H)^{-1}$ is the pseudo-inverse of $\tilde{\mathbf{H}}$. In Proposition 2, we suppose for simplicity $\mathbf{Q} = \mathbf{I}_2$, although the generalization is straightforward. When $M_1 \rightarrow \infty$, as in Sect. VI-A, $\mathbf{V}^{(1)}$ tends to a unitary matrix, so that, similarly to (34), $\|\tilde{\mathbf{H}}^+\|_{\text{F}}^2 \xrightarrow{M_1 \rightarrow \infty} \text{Tr} \left\{ \left(\tilde{\mathbf{M}} \tilde{\mathbf{M}}^H \right)^{-1} \right\}$.

³Here, in order to handle complex differentiation of non analytic functions we use the definition of Wirtinger derivatives [39].

For $L_n \rightarrow \infty$, the spatial signatures $\{\mathbf{u}_{k,n}^{(2)}\}_{k,n=1}^2$ become orthogonal, provided that all users are angularly separated. Thus, for IRS n , the space of useful signal is the bidimensional space spanned by the orthonormal basis $\{\mathbf{u}_{1,n}^{(2)}, \mathbf{u}_{2,n}^{(2)}\}$. So, we can write $\tilde{\mathbf{u}}_n$ as

$$\tilde{\mathbf{u}}_n = \cos \theta_n \cos \phi_n \mathbf{u}_{1,n}^{(2)} + \cos \theta_n \sin \phi_n \mathbf{u}_{2,n}^{(2)} + \tilde{\mathbf{u}}_n^\perp \quad (48)$$

where $\tilde{\mathbf{u}}_n^\perp$ is the component of $\tilde{\mathbf{u}}_n$ orthogonal to the useful signal space. Defining $\gamma_n = \cos \theta_n$, $\kappa_n = \cos \phi_n$, $\sigma_n = \sin \phi_n$ and $\mu_{k,n} = |t_{k,n}|$, we can reformulate the optimization problem as the maximization of function f given by

$$f = \text{Tr} \left\{ \left(\widetilde{\mathbf{M}} \widetilde{\mathbf{M}}^H \right)^{-1} \right\}^{-1} = \frac{(\mu_{11}\mu_{22}\kappa_1\sigma_2 - \mu_{12}\mu_{21}\sigma_1\kappa_2)^2}{1/\gamma_1^2(\mu_{11}^2\kappa_1^2 + \mu_{21}^2\sigma_1^2) + 1/\gamma_2^2(\mu_{12}^2\kappa_2^2 + \mu_{22}^2\sigma_2^2)}. \quad (49)$$

Now, we solve the optimization problem without considering the equimodular condition on $\tilde{\mathbf{u}}_n$. First, the maximum of f is obtained for $\gamma_1 = \gamma_2 = 1$, i.e., $\tilde{\mathbf{u}}_n$ belongs to the useful signal space, a pretty obvious fact. To maximize f with respect to ϕ_n , $n = 1, 2$, we set the gradient ∇f to zero. Writing $f = f_1/f_2$, we have for $n = 1, 2$

$$\frac{\partial f}{\partial \phi_n} = \frac{\partial f_1}{\partial \phi_n} \frac{1}{f_2} - \frac{\partial f_2}{\partial \phi_n} \frac{f_1}{f_2^2} = 0 \implies \frac{\partial f_1}{\partial \phi_n} = \frac{\partial f_2}{\partial \phi_n} \frac{f_1}{f_2}.$$

We obtain the following two equations (for $f_1 > 0$, since $f_1 = 0$ gives a minimum of f):

$$\begin{aligned} \mu_{12}\mu_{21}\sigma_1\sigma_2(\mu_{22}^2 + \zeta_1) + \mu_{11}\mu_{22}\kappa_1\kappa_2(\mu_{12}^2 + \zeta_1) &= 0 \\ \mu_{11}\mu_{22}\sigma_1\sigma_2(\mu_{21}^2 + \zeta_2) + \mu_{12}\mu_{21}\kappa_1\kappa_2(\mu_{11}^2 + \zeta_2) &= 0. \end{aligned}$$

having defined $\zeta_1 = \mu_{11}^2\kappa_1^2 + \mu_{21}^2\sigma_1^2$ and $\zeta_2 = \mu_{12}^2\kappa_2^2 + \mu_{22}^2\sigma_2^2$. The above equations are satisfied if $\sigma_1\sigma_2 = 0$ and $\kappa_1\kappa_2 = 0$. This yields two points in the first quadrant, i.e. $(\phi_1, \phi_2) = (0, \pi/2)$ and $(\phi_1, \phi_2) = (\pi/2, 0)$. The first point corresponds to assigning user 1 to IRS 1 and user 2 to IRS 2, while the second assigns user 2 to IRS 1 and user 1 to IRS 2. Instead, if $\sigma_1\sigma_2 \neq 0$ and $\kappa_1\kappa_2 \neq 0$, we can solve both equations above for $\frac{\sigma_1\sigma_2}{\kappa_1\kappa_2}$ and equate the solutions. By doing this, after a little bookkeeping, we obtain the following equation:

$$\mu_{11}^2\mu_{21}^2(\mu_{22}^2 - \mu_{12}^2)\zeta_1 + \mu_{12}^2\mu_{22}^2(\mu_{11}^2 - \mu_{21}^2)\zeta_2 + (\mu_{11}^2\mu_{22}^2 - \mu_{21}^2\mu_{12}^2)\zeta_1\zeta_2 = 0$$

But, if $\mu_{11} > \mu_{21}$ and $\mu_{22} > \mu_{12}$, all coefficients of ζ_1 and ζ_2 are positive and, since $\zeta_n > 0$, $n = 1, 2$, the above equation does not have any solution. Analogously if $\mu_{11} < \mu_{21}$ and $\mu_{22} < \mu_{12}$. Thus, in such conditions, the only two stationary points are those corresponding to IRS-user assignments, and one of the two must be the global maximum. The global maximum is the first point if

$$\frac{1}{\mu_{11}^2} + \frac{1}{\mu_{22}^2} < \frac{1}{\mu_{12}^2} + \frac{1}{\mu_{21}^2}$$

otherwise the global maximum is the second point. The obtained optimal IRS phase shifts are equal to the solution of the optimization problem in (37).

REFERENCES

- [1] J. Qiao and M.-S. Alouini, "Secure transmission for intelligent reflecting surface-assisted mmwave and terahertz systems," *IEEE Wireless Communications Letters*, vol. 9, no. 10, pp. 1743–1747, Sept. 2020.
- [2] I. F. Akyildiz, J. M. Jornet, and C. Han, "Terahertz band: Next frontier for wireless communications," *Physical Communication*, vol. 12, pp. 16–32, 2014.
- [3] M. Di Renzo *et al.*, "Smart radio environments empowered by reconfigurable AI meta-surfaces: an idea whose time has come," *EURASIP Journal Wireless Communication Networks*, vol. 129, May 2019.
- [4] Q. Wu and R. Zhang, "Towards smart and reconfigurable environment: Intelligent reflecting surface aided wireless network," *IEEE Communications Magazine*, pp. 106–112, January 2020.
- [5] C. Liaskos, S. Nie, A. Tsioliaridou, A. Pitsillides, S. Ioannidis, and I. Akyildiz, "A new wireless communication paradigm through software-controlled metasurfaces," *IEEE Comm. Magazine*, vol. 56, no. 9, pp. 162–169, Sept. 2018.
- [6] Z. Zhang, L. Dai, X. Chen, C. Liu, F. Yang, R. Schober, and H. V. Poor, "Active RIS vs. passive RIS: Which will prevail in 6G?" 2022. [Online]. Available: <https://arxiv.org/abs/2103.15154>
- [7] M. A. ElMossallamy, H. Zhang, L. Song, K. G. Seddik, Z. Han, and G. Y. Li, "Reconfigurable intelligent surfaces for wireless communications: Principles, challenges, and opportunities," *IEEE Transactions on Cognitive Communications and Networking*, vol. 6, no. 3, pp. 990–1002, 2020.
- [8] S. Gong, X. Lu, D. T. Hoang, D. Niyato, L. Shu, D. I. Kim, and Y.-C. Liang, "Toward smart wireless communications via intelligent reflecting surfaces: A contemporary survey," *IEEE Communications Surveys Tutorials*, vol. 22, no. 4, pp. 2283–2314, Apr. 2020.
- [9] Q. Wu, S. Zhang, B. Zheng, C. You, and R. Zhang, "Intelligent reflecting surface-aided wireless communications: A tutorial," *IEEE Transactions on Communications*, vol. 69, no. 5, pp. 3313–3351, May 2021.
- [10] M. A. Saeidi, M. J. Emadi, H. Masoumi, M. R. Mili, D. W. K. Ng, and I. Krikidis, "Weighted sum-rate maximization for multi-IRS-assisted full-duplex systems with hardware impairments," *IEEE Transactions on Cognitive Communications and Networking*, vol. 7, no. 2, Feb. 2021.
- [11] C. Pan, H. Ren, K. Wang, W. Xu, M. ElKashlan, A. Nallanathan, and L. Hanzo, "Multicell MIMO communications relying on intelligent reflecting surfaces," *IEEE Trans. on Wireless Comm.*, vol. 19, no. 8, pp. 5218–5232, Aug. 2020.
- [12] Z. Li, M. Hua, Q. Wang, and Q. Song, "Weighted sum-rate maximization for multi-IRS aided cooperative transmission," *IEEE Wireless Communications Letters*, vol. 9, no. 10, pp. 1620–1624, Oct. 2020.
- [13] C. Liaskos, A. Tsioliaridou, A. Pitsillides, S. Ioannidis, and I. Akyildiz, "Using any surface to realize a new paradigm for wireless communications," 2018. [Online]. Available: <https://arxiv.org/abs/1806.04585>
- [14] M. H. Alsharif, A. H. Kelechi, M. A. Albreem, S. A. Chaudhry, M. S. Zia, and S. Kim, "Sixth generation (6G) wireless networks: Vision, research activities, challenges and potential solutions," *Symmetry*, vol. 12, no. 4, Apr. 2020. [Online]. Available: <https://www.mdpi.com/2073-8994/12/4/676>
- [15] X. Tan, Z. Sun, J. M. Jornet, and D. Pados, "Increasing indoor spectrum sharing capacity using smart reflect-array," in *2016 IEEE International Conference on Communications (ICC)*, 2016, pp. 1–6.
- [16] Y. Pan, K. Wang, C. Pan, H. Zhu, and J. Wang, "Sum-rate maximization for intelligent reflecting surface assisted terahertz communications," *IEEE Transactions on Vehicular Technology*, (Early Access), 2022.
- [17] Q. Wu and R. Zhang, "Intelligent reflecting surface enhanced wireless network: Joint active and passive beamforming design," Sep. 2018. [Online]. Available: <https://arxiv.org/abs/1809.01423>
- [18] M.-M. Zhao, Q. Wu, M.-J. Zhao, and R. Zhang, "Intelligent reflecting surface enhanced wireless networks: Two-timescale beamforming optimization," *IEEE Trans. on Wireless Communications*, vol. 20, no. 1, pp. 2–17, Jan. 2021.
- [19] P. Wang, J. Fang, X. Yuan, Z. Chen, and H. Li, "Intelligent reflecting surface-assisted millimeter wave communications: Joint active and passive precoding design," *IEEE Transactions on Vehicular Technology*, vol. 69, no. 12, pp. 14960–14973, Dec. 2020.

- [20] X. Li, J. Fang, F. Gao, and H. Li, "Joint active and passive beamforming for intelligent reflecting surface-assisted massive MIMO systems," 2019. [Online]. Available: <https://arxiv.org/abs/1912.00728>
- [21] C. Han, J. M. Jornet, and I. Akyildiz, "Ultra-massive mimo channel modeling for graphene-enabled terahertz-band communications," in *2018 IEEE 87th Vehicular Technology Conference (VTC Spring)*, 2018, pp. 1–5.
- [22] S. Tarboush, H. Sardeddeen, H. Chen, M. H. Loukil, H. Jemaa, M. S. Alouini, and T. Y. Al-Naffouri, "TeraMIMO: A channel simulator for wideband ultra-massive MIMO terahertz communications," 2021. [Online]. Available: <https://arxiv.org/abs/2104.11054>
- [23] Y. Xing, O. Kanhere, S. Ju, and T. S. Rappaport, "Indoor wireless channel properties at millimeter wave and sub-terahertz frequencies," 2019. [Online]. Available: <https://arxiv.org/abs/1908.09765>
- [24] O. Özdoğan, E. Björnson, and E. G. Larsson, "Intelligent reflecting surfaces: Physics, propagation, and pathloss modeling," *IEEE Wireless Communications Letters*, vol. 9, no. 5, pp. 581–585, May 2020.
- [25] J. He, H. Wymeersch, L. Kong, O. Silvén, and M. Juntti, "Large intelligent surface for positioning in millimeter wave MIMO systems," in *2020 IEEE 91st Vehicular Technology Conference (VTC2020-Spring)*, 2020, pp. 1–5.
- [26] A. Tarable, F. Malandrino, L. Dossi, R. Nebuloni, G. Virone, and A. Nordin, "Meta-surface optimization in 6G sub-THz communications," in *2020 IEEE International Conference on Communications Workshops*, 2020, pp. 1–6.
- [27] M. Dunna, C. Zhang, D. Sievenpiper, and D. Bharadia, "ScatterMIMO: Enabling virtual MIMO with smart surfaces," *MobiCom '20: Proceedings of the 26th Annual International Conference on Mobile Computing and Networking*, no. 10, pp. 1–14, Oct. 2020.
- [28] 3GPP, "5G; Study on Channel Model for Frequencies from 0.5 to 100 GHz - Release 14," 3rd Generation Partnership Project (3GPP), Tech. Rep. 38.901, 2017.
- [29] J. Kokkonen, J. Lehtomäki, and M. Juntti, "Simple molecular absorption loss model for 200–450 gigahertz frequency band," in *2019 European Conference on Networks and Communications (EuCNC)*, 2019, pp. 219–223.
- [30] S. Abeywickrama, R. Zhang, and C. Yuen, "Intelligent reflecting surface: Practical phase shift model and beamforming optimization," in *ICC 2020 - 2020 IEEE International Conference on Communications (ICC)*, 2020, pp. 1–6.
- [31] W. Tang, M. Z. Chen, X. Chen, J. Y. Dai, Y. Han, M. Di Renzo, Y. Zeng, S. Jin, Q. Cheng, and T. J. Cui, "Wireless communications with reconfigurable intelligent surface: Path loss modeling and experimental measurement," *IEEE Transactions on Wireless Communications*, vol. 20, no. 1, p. 421–439, Jan 2021.
- [32] M. Di Renzo, F. Habibi Danufane, X. Xi, J. de Rosny, and S. Tretyakov, "Analytical modeling of the path-loss for reconfigurable intelligent surfaces – anomalous mirror or scatterer?" in *2020 IEEE 21st International Workshop on Signal Processing Advances in Wireless Communications (SPAWC)*, 2020, pp. 1–5.
- [33] J. Xu, W. Xu, and A. L. Swindlehurst, "Discrete phase shift design for practical large intelligent surface communication," in *IEEE Pacific Rim Conference on Communications, Computers and Signal Processing*, 2019, pp. 1–5.
- [34] Q. Wu and R. Zhang, "Beamforming optimization for wireless network aided by intelligent reflecting surface with discrete phase shifts," *IEEE Transactions on Communications*, vol. 68, no. 3, pp. 1838–1851, 2020.
- [35] ———, "Intelligent reflecting surface enhanced wireless network via joint active and passive beamforming," *IEEE Transactions on Wireless Communications*, vol. 18, no. 11, pp. 5394–5409, Nov. 2019.
- [36] C. Huang, A. Zappone, G. C. Alexandropoulos, M. Debbah, and C. Yuen, "Reconfigurable intelligent surfaces for energy efficiency in wireless communication," *IEEE Transactions on Wireless Communications*, vol. 18, no. 8, pp. 4157–4170, Aug. 2019.
- [37] H. W. Kuhn, "The hungarian method for the assignment problem," *Naval Research Logistics Quarterly*, vol. 2, no. 1–2, pp. 83–97, 1955.
- [38] K. B. Petersen, M. S. Pedersen, J. Larsen, K. Strimmer, L. Christiansen, K. Hansen, L. He, L. Thibaut, M. Baro, S. Hattinger *et al.*, "The matrix cookbook," *Kgs. Lyngby, Denmark: Tech. Univ. Denmark*, 2006.
- [39] R. Remmert, *Theory of Complex Functions*. Springer-Verlag, 1998.